

University of Groningen

Computational spectroscopy of complex systems

Jansen, Thomas L.C.

Published in:
Journal of Chemical Physics

DOI:
[10.1063/5.0064092](https://doi.org/10.1063/5.0064092)

IMPORTANT NOTE: You are advised to consult the publisher's version (publisher's PDF) if you wish to cite from it. Please check the document version below.

Document Version
Publisher's PDF, also known as Version of record

Publication date:
2021

[Link to publication in University of Groningen/UMCG research database](#)

Citation for published version (APA):

Jansen, T. L. C. (2021). Computational spectroscopy of complex systems. *Journal of Chemical Physics*, 155(17), [170901]. <https://doi.org/10.1063/5.0064092>

Copyright

Other than for strictly personal use, it is not permitted to download or to forward/distribute the text or part of it without the consent of the author(s) and/or copyright holder(s), unless the work is under an open content license (like Creative Commons).

The publication may also be distributed here under the terms of Article 25fa of the Dutch Copyright Act, indicated by the "Taverne" license. More information can be found on the University of Groningen website: <https://www.rug.nl/library/open-access/self-archiving-pure/taverne-amendment>.

Take-down policy

If you believe that this document breaches copyright please contact us providing details, and we will remove access to the work immediately and investigate your claim.

Downloaded from the University of Groningen/UMCG research database (Pure): <http://www.rug.nl/research/portal>. For technical reasons the number of authors shown on this cover page is limited to 10 maximum.


Computational spectroscopy of complex systems

Cite as: J. Chem. Phys. **155**, 170901 (2021); <https://doi.org/10.1063/5.0064092>

Submitted: 20 July 2021 • Accepted: 13 September 2021 • Published Online: 01 November 2021

 Thomas L. C. Jansen

COLLECTIONS

 This paper was selected as Featured



View Online



Export Citation



CrossMark

ARTICLES YOU MAY BE INTERESTED IN

[The momentum of models](#)

The Journal of Chemical Physics **155**, 170902 (2021); <https://doi.org/10.1063/5.0023891>

[Chemical physics software](#)

The Journal of Chemical Physics **155**, 010401 (2021); <https://doi.org/10.1063/5.0059886>

[Perspective on integrating machine learning into computational chemistry and materials science](#)

The Journal of Chemical Physics **154**, 230903 (2021); <https://doi.org/10.1063/5.0047760>

The Journal
of Chemical Physics

SPECIAL TOPIC: Low-Dimensional
Materials for Quantum Information Science

Submit Today!

Computational spectroscopy of complex systems

Cite as: *J. Chem. Phys.* **155**, 170901 (2021); doi: [10.1063/5.0064092](https://doi.org/10.1063/5.0064092)

Submitted: 20 July 2021 • Accepted: 13 September 2021 •

Published Online: 1 November 2021




View Online



Export Citation



CrossMark

Thomas L. C. Jansen^{a)} 

AFFILIATIONS

Zernike Institute for Advanced Materials, University of Groningen, Nijenborgh 4, 9747 AG Groningen, The Netherlands

^{a)} Author to whom correspondence should be addressed: t.l.c.jansen@rug.nl

ABSTRACT

Numerous linear and non-linear spectroscopic techniques have been developed to elucidate structural and functional information of complex systems ranging from natural systems, such as proteins and light-harvesting systems, to synthetic systems, such as solar cell materials and light-emitting diodes. The obtained experimental data can be challenging to interpret due to the complexity and potential overlapping spectral signatures. Therefore, computational spectroscopy plays a crucial role in the interpretation and understanding of spectral observables of complex systems. Computational modeling of various spectroscopic techniques has seen significant developments in the past decade, when it comes to the systems that can be addressed, the size and complexity of the sample types, the accuracy of the methods, and the spectroscopic techniques that can be addressed. In this Perspective, I will review the computational spectroscopy methods that have been developed and applied for infrared and visible spectroscopies in the condensed phase. I will discuss some of the questions that this has allowed answering. Finally, I will discuss current and future challenges and how these may be addressed.

Published under an exclusive license by AIP Publishing. <https://doi.org/10.1063/5.0064092>

I. INTRODUCTION

Characterization of the functional properties of biological systems and man-made structures and devices is crucial for achieving a fundamental understanding of the underlying principles of the function and for the design of new and improved functional materials.^{1–4} Spectroscopic characterization methods are generally very powerful as they often allow for high spatial^{5–7} and time resolution,^{8,9} limited sample damage,⁷ and few restrictions on sample preparation.^{7,10,11} Current applications go far beyond the application of spectroscopy to characterize single atoms or molecules. Very complex systems with diverse functions can be characterized. Still, the spectroscopic observables may be very challenging to interpret due to broad line shapes and the intrinsic heterogeneity of complex systems.^{12–14} Therefore, spectral modeling and computation are of paramount importance to unravel the underlying physical properties and functions being the intricate spectroscopic observables. In this Perspective, I will discuss some of the progress made in recent years with the focus on the procedure, which can be used to go from proposed structures to predicted spectra and spectral interpretation and assignment.

High-level quantum chemistry calculations are required for the calculation of the spectroscopy of atoms¹⁵ and molecules¹⁶ in the gas phase. This can be done as typically, the systems of interest

are small and the number of degrees of freedom is limited. In the condensed phase, the environment cannot be neglected, and understanding the spectral variation depending on the change in packing, solvation, and specific interactions is often of main interest. While continuum solvent models^{17,18} may be sufficient to describe the average situation in solution, such models cannot take the dynamic effects and specific binding into account. For this, spectral calculations including the explicit environment are needed.^{19–25} This level of theory can be very well suited for understanding absorption spectroscopy of molecular chromophores both in solution and in complex condensed phase scaffolds. However, such techniques are still computationally too demanding to explicitly model time-resolved spectroscopies and extended systems with numerous coupled chromophores. Therefore, special techniques have been developed to predict excited state solvent shifts^{26,27} of molecules in the condensed phase and couplings^{28,29} between those at a speed sufficient enough to be used in quantum–classical response function based spectral calculations.^{30,31} Such calculations provide the possibility of predicting and interpreting advanced spectroscopies as two-dimensional (2D) infrared³² and electronic spectroscopies³³ of complex systems containing tens or even hundreds of chromophores.^{34,35} This kind of computational spectroscopy of complex systems is needed for the interpretation of experimental spectra, design of new materials, and prediction of spectral properties.

The remainder of this Perspective is organized as follows: First, the quantum–classical procedure used to calculate the spectra of complex systems is outlined in Sec. II. This will be followed by examples of applications to vibrational and electronic spectroscopies in Secs. III and IV, respectively. Finally, a concluding discussion including a perspective of future directions will be presented in Sec. V.

II. QUANTUM–CLASSICAL PROCEDURE

Typically, computational spectroscopy of complex systems requires the use of a quantum–classical procedure, where degrees of freedom not observed directly in the spectra are treated using classical dynamics and the degrees of freedom involved directly in the spectroscopy are treated quantum mechanically. In Fig. 1, I outline a typical workflow for a quantum–classical procedure to obtain and interpret spectra of complex systems. The elements of the procedure starting with an initial guess structure of a system of interest and ending with tests against experimental data and potential improvement of the proposed structure and analysis of the predicted functional properties are discussed in detail in this section.

A. Initial structure

The first step is to predict a structure for the system of interest. In some cases, initial atomistic structures can be based on x-ray, nuclear magnetic resonance (NMR), or electron microscopy

experiments. For biological systems, structures can, for example, be found in the Protein Data Bank.³⁶ In other cases, one has to rely on guessing based on the limited information available, and the structure may be refined by successive calculation of spectra with different guess structures and comparison of the resulting spectra with experimental data. For proteins with unknown structures, such guess could, for example, come from protein folding prediction software such as AlphaFold2.³⁷ In this way, computational spectroscopy may, thus, help find a structural subspace with structures consistent with spectroscopic observations.

B. Molecular dynamics

Spectra can be determined for static structures; however, molecular dynamics provide a tool to predict dynamics from the femtosecond time scale up to microseconds. Since most systems are flexible or exhibit functional dynamics, this is often a crucial part of a computational spectroscopy simulation. The initial structure is allowed to move according to Newtonian dynamics under a set of assumptions. The most important assumption is that the particles in the structure, which are typically atoms, are assumed to feel each other with a given set of interactions defined by a force field. These force fields are typically parameterized based on a combination of quantum chemistry calculations and empirical fitting. For systems such as water and proteins, numerous force fields^{38–42} exist, and one can choose depending on experience and preference. For less

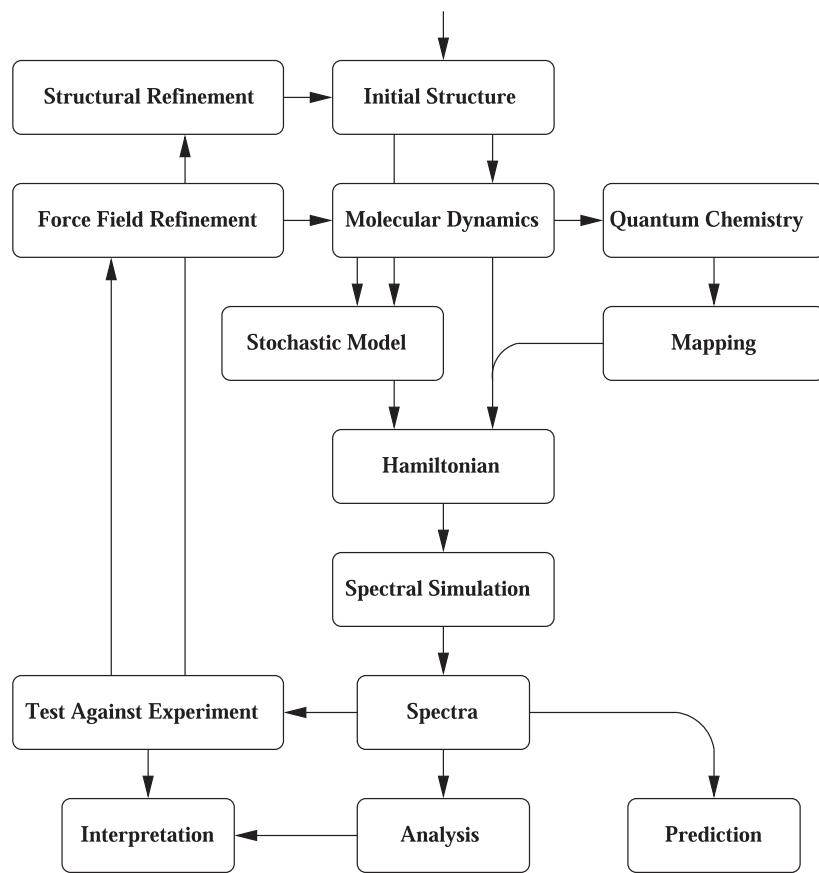


FIG. 1. An overview of the typical elements in the workflow for computational spectroscopy.

common systems, one will need to develop a force field for the system before molecular dynamics simulations can be performed. For very large systems, coarse grained simulations where groups of atoms that are treated together as beads may allow simulations on time scales beyond the microsecond, which may be relevant especially for large complex systems. Backmapping procedures⁴³ exist to retrieve the atomistic positions, which may be needed for further spectroscopic predictions.

C. Hamiltonian

For many complex systems, a multi-chromophoric Frenkel exciton type Hamiltonian can be used.⁴⁴ In essence, each of the N chromophores is then expected to behave like a two-level or a three-level system. These two general pictures are illustrated in Fig. 2. The states in each chromophore are coupled to those in the other chromophores through a pairwise coupling term. This multi-chromophoric basis results in a global ground state, a single excited state manifold, and manifolds with multiple excitations in the system. For simplicity, I will, only explicitly, consider the three lowest excitation manifolds as these are sufficient to describe many spectroscopic techniques including two-dimensional spectroscopies. A general form of the Hamiltonian trajectory is^{32,45}

$$H(t) = \sum_n \epsilon_n(t) B_n^\dagger B_n - \frac{1}{2} \sum_n \Delta_n(t) B_n^\dagger B_n^\dagger B_n B_n + \sum_{n,m} J_{nm}(t) B_n^\dagger B_m - \sum_n \vec{E}(t) \cdot \vec{\mu}_n(t) [B_n^\dagger + B_n]. \quad (1)$$

Here, B_n^\dagger and B_n are creation and annihilation operators. For vibrational spectroscopy, these operators are Bosonic, reflecting the harmonic basis,³² while they are Paulionic for electronic systems, reflecting the two-level nature of the excitations.⁴⁵ The energy gap between the chromophore ground and first excited states on chromophore n is $\epsilon_n(t)$. The coupling strength of chromophore n with

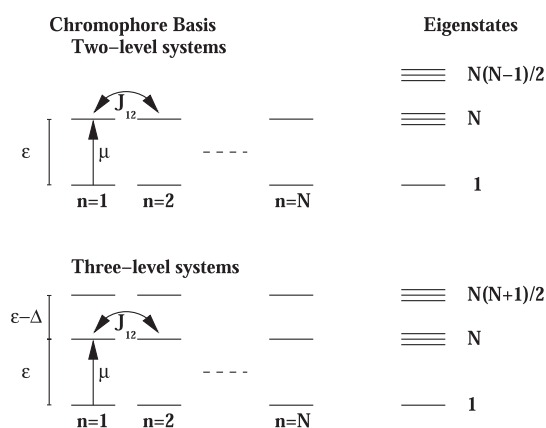


FIG. 2. Illustration of the energy levels as used in computational spectroscopy of multi-chromophoric systems. (Left) The site basis is illustrated for two- and three-level systems, while the resulting eigenstate manifolds are illustrated on the right. The vertical arrows illustrate the transition between the ground and excited states induced by an external electric field. The bend double-headed arrows illustrate couplings between different sites. The symbols are defined in the text and in Eq. (1).

the external electric field, $\vec{E}(t)$, is determined by the transition dipole, $\vec{\mu}_n(t)$. In the case of a three-level description, the anharmonicity, $\Delta_n(t)$, defines the difference of the energy gap between the first and second excited states as compared to the gap between the ground and first excited states. The anharmonicity is defined to be positive if the former gap is smaller than the latter. In the case of coupled three-level systems, the Hamiltonian given above gives transition strengths and couplings between the different states in the manifold of second excited states according to harmonic rules. For example, the transition dipole between the first excited and the second excited state of a chromophore is $\sqrt{2}$ times the transition-dipole strength of the transition between the ground and the first excited state. Further generalizations to this picture exist,^{46,47} but will not be discussed further here. For two-level systems, the anharmonic term is left out, and basis states with multiple excitations on the same chromophore are left out from the calculations. This results in $N(N-1)/2$ states with two excitations in the system. In contrast, a collection of three-level systems has $N(N+2)/2$ states with two excitations. The double excited states play an important role in non-linear spectroscopies such as pump-probe and two-dimensional spectroscopies. Typically, the three-level system description applies to vibrational spectroscopy and the two-level system description to electronic spectroscopy.⁴⁸

D. Quantum chemistry

The effect of solvent and molecular configurations on the quantum transitions observed in spectra can be obtained with quantum chemical calculations using explicit or implicit solvent calculations. For modeling the effect of explicit solvent dynamics, explicit solvent modeling is needed. In principle, it is possible to calculate the parameters in Eq. (1) for explicit solvent configurations of the chromophores along a molecular dynamics trajectory. However, such treatment is typically limited to relatively cheap semi-empirical methods^{34,49} or time-dependent density functional theory (DFT) calculations^{50–54} for very short trajectories. Only for very small systems, it is meaningful to use high-quality correlated quantum chemical methods.²⁵ The couplings between pairs of molecules can be obtained from explicit calculations on dimers. This is, however, even more time consuming especially if there are many chromophore pairs. These approaches are, therefore, effectively limited to systems with 20–50 chromophores.

E. Mapping

As outlined above, performing quantum chemical calculations for thousands of time steps along a molecular dynamics trajectory is very time consuming. A powerful alternative is to create a mapping of the transition energies and dipoles⁵⁵ based on quantum chemical calculations on a subset of typical structural configurations. For vibrational modes, DFT calculations of the molecule of interest, such as water or *N*-methyl acetamide, were performed in point charge environments or solvated clusters extracted from molecular dynamics simulations. Assuming that the solvent shift was mainly of electrostatic nature, fits were then made assuming that the vibrational frequency could be described in as a weighted sum of electrostatic potential, fields, and field gradients from the surrounding solvent molecules on atoms involved in the vibration.^{56–62}

This strategy was found to perform well for many vibrations at least in polar solvents.⁵⁵ For electronic transitions, the excitation energies were modeled by extracting atomistic charges for the ground state as well as of the excited state.⁶³ The solvent shift was then calculated as the change in the Coulomb interaction energy between the dye molecule and the surrounding solvent when calculated with the excited state and ground state charges. At an additional level of theory, the effect of the polarizability of the solvent was included.^{64,65}

For couplings between different states, vibrational or electronic, the simplest approximation is the transition-dipole coupling, which is accurate when the distance between the chromophores is larger than their individual size. The transition-dipole coupling is then^{66,67}

$$J_{nm} = \frac{1}{4\pi\epsilon_0} \left(\frac{\vec{\mu}_n \cdot \vec{\mu}_m}{r_{nm}^3} - 3 \frac{\vec{\mu}_n \cdot \vec{r}_{nm} \vec{\mu}_m \cdot \vec{r}_{nm}}{r_{nm}^5} \right), \quad (2)$$

where $\vec{\mu}_n$ is the transition dipole for a given transition and r_{nm} is the distance between the center of the chromophores. Further extensions to the extended dipole, transition charge coupling,²⁹ and transition density cube methods⁶⁸ accounting for multipole effects⁶⁶ in the coupling are possible.

F. Stochastic model

Stochastic models can be a useful tool for modeling the dynamics of the structure and parameters in the Hamiltonian in Eq. (1). This can be because explicit structural information is not known, the research question at hand may not require an atomistic model, or the mapping approach outlined above may be too time consuming for very large systems. Typical stochastic models are designed to reproduce the auto-correlation function of the energy-gap fluctuations, $C(t) = \langle \epsilon_n(t) \epsilon_n(0) \rangle$, or the corresponding spectral density, $D(\omega)$. The two properties are related through the identities:⁶⁹

$$D(\omega) = D_{\text{even}}(\omega) + D_{\text{odd}}(\omega), \quad (3)$$

$$D_{\text{even}}(\omega) = D_{\text{odd}}(\omega) \coth(\hbar\omega/2k_B T), \quad (4)$$

$$C_Q(t) = \int_{-\infty}^{\infty} d\omega \cos(\omega t) \coth(\hbar\omega/2k_B T) D_{\text{odd}}(\omega) + i \int_{-\infty}^{\infty} d\omega \sin(\omega t) D_{\text{odd}}(\omega). \quad (5)$$

The second equation is the fluctuation–dissipation theorem relating the even and odd parts of the spectral density. The third equation defines the energy-gap quantum correlation function in terms of the odd part of the spectral density. For a harmonic bath, the spectral density D_{odd} tells which frequencies are available in the bath and how strongly they modulate the energy gap in the system. Under the harmonic bath assumption and the assumption of the linear coupling between the bath and the system, D_{odd} is independent of temperature, the stochastic process described is a Gaussian process,^{70–72} and the auto-correlation function (or equivalently the spectral density) fully characterizes the system–bath interaction. The real part of the quantum correlation function, $C_Q(t)$, is typically approximated using the purely real classical energy-gap auto-correlation function, which is trivially retrieved from the trajectory of the energy gap.⁶⁹

For small values of $\hbar\omega/2k_B T$ (high-temperature), the coth term can be approximated by $2k_B T/\hbar\omega$, and the imaginary part becomes much smaller than the real part.

The parameters for a stochastic model may be based on experimental data, where knowledge about the time scale of energy-gap fluctuations is known, experiments providing an approximate spectral density, or by fitting experimental spectral shapes. Alternatively, the parameters may be based on quantum chemical or mapping calculations on a subset of the chromophores. In the latter case, it is typically a good approximation that the energy-gap fluctuations in different chromophores, even in close spatial proximity, are uncorrelated.⁷³ This significantly simplifies the treatment as the chromophore fluctuations of different chromophores can be treated independently. The overdamped Brownian oscillator model is often sufficient for modeling line shapes and with only two free parameters preventing overfitting. For this model,

$$D_{\text{odd}}(\omega) = 2\lambda \frac{\omega\Lambda}{\omega^2 + \Lambda^2}, \quad (6)$$

and the classical correlation function is $C_C(t) = \langle \epsilon(t) \epsilon(0) \rangle = \sigma^2 \exp(-\Lambda t)$, where the reorganization energy, λ , and the magnitude of the frequency fluctuations, σ , are related by $\sigma^2 = 2\lambda k_B T$. In electronic spectroscopy, the reorganization energy is directly related to the observable Stokes shift, which is challenging to observe in vibrational spectroscopy.^{74,75} Energy-gap trajectories describing overdamped Brownian oscillator behavior are easy to generate.^{76,77} Multiple spectral densities can also be combined treating the overall spectral density as a sum of different components originating from different bath degrees of freedom. The use of the overdamped Brownian oscillator here is intended as a simple example, and for specific systems, other functional forms may be required^{54,78,79} or computationally advantageous.⁸⁰ It is important to realize that different expressions and definitions for the spectral density exist in the literature, depending on choices of units and definitions of the Fourier transform.

In practice, a number of systems have been reported to exhibit non-Gaussian dynamics,^{34,81–87} and these, thus, cannot be described by a spectral density. This breakdown was found to arise from the non-linear system–bath coupling as molecular interactions typically depend on electric fields and/or potentials,⁸⁶ which exhibit non-linear dependence on the molecular distances. At the same time at finite temperatures, anharmonic parts of the bath potential energy surface become accessible. While the spectral density in theory is temperature independent, in practice, a spectral density determined at one temperature can only be used at another temperature if the system is harmonic.

G. Spectral simulations

A number of general purpose spectral simulation programs taking Frenkel type Hamiltonian trajectories as input exist. These include the SPECTRON⁸⁸ and numerical integration of the Schrödinger equation (NISE)^{89,90} codes, which have both been optimized to allow efficient simulation of a variety of spectroscopic signals for extended systems. A wide variety of approximations exist for simulating the spectra. A complete overview of these is beyond the scope of this Perspective. Here, I will consider the simple sum-over states approach, the second-order cumulant

approach,^{71,91} the numerical integration of the Schrödinger equation (NISE) approach,^{92,93} and the Hierarchical Equations of Motion Approach (HEOM).^{79,94–96}

In the sum-over states approach, the Hamiltonian of Eq. (1) is diagonalized, and Fermi's golden rule⁹⁷ type expressions are used to obtain the spectra. For disordered systems, the spectra are averaged over numerous different Hamiltonians corresponding to different disorder realizations. As an example, the absorption spectrum is given by

$$I(\omega) = \left\langle \sum_i |\bar{\mu}_i|^2 L(\omega - \lambda_i) \right\rangle. \quad (7)$$

Here, ω is the frequency of the absorption and $\langle \dots \rangle$ denotes the ensemble average. $\bar{\mu}_i$ is the transition dipole associated with eigenstate i and λ_i is the eigenvalue associated with the same eigenstate. The function $L(\omega)$ describes the line shape of each absorption line and is typically chosen as a Lorentzian function with a width associated with the lifetime or homogeneous linewidth of the transition. The expressions for other spectroscopic techniques can be found in various textbooks.^{69,98–100} The sum-over states approximation is generally easy to apply, but it does not account for phenomena such as spectral diffusion and motional narrowing.

The second-order cumulant approximation is based on the assumption that the system–bath fluctuations are fully described by the spectral density. Under this assumption, the exact line shape of each individual transition can be predicted using the so-called line shape function here expressed in terms of the frequency correlation function,

$$g(t) = \int_0^t \int_0^{\tau'} d\tau' d\tau'' C(\tau''). \quad (8)$$

The absorption spectrum in this case is given by

$$I(\omega) = \sum_j |\bar{\mu}_j|^2 \Re \int_0^\infty \exp(-i(\omega - \langle \lambda_j \rangle)t) \exp(-g_j(t)) dt. \quad (9)$$

Here, $g_j(t)$ is the line shape function associated with eigenstate j , which has the average eigenvalue $\langle \lambda_j \rangle$. The ensemble averaging in this expression is moved from an average of the full expression as given in Eq. (7) to an ensemble average in the classical correlation function. In the case of an overdamped Brownian oscillator correlation function, the line shape function is^{69,71}

$$g(t) = \frac{\sigma^2}{\Lambda^2} \left(1 - i \frac{\Lambda}{2k_B T} \right) (\exp(-\Lambda t) + \Lambda t - 1). \quad (10)$$

In the fast modulation limit ($\Lambda \gg \sigma$), this expression leads to Lorentzian line shapes, and in the slow modulation limit ($\Lambda \ll \sigma$), Gaussian line shapes are obtained. The expression is, however, also exact for the intermediate regime. Furthermore, this approach accounts for the bath relaxation responsible for the Stokes shift in fluorescence spectra as reflected by the imaginary term in Eq. (10). The ensemble average in the second-order cumulant expression does not include an average over transition-dipole moment, and if the transition-dipole moment fluctuates, this so-called non-Condon effect¹⁰⁰ is, thus, not accounted for. This effect is very pronounced for the OH-stretch vibration in, for example, water, where the transition dipole varies by a factor of 5 across the spectral width of the band.¹⁰¹ This effect is responsible for the Raman non-coincidence

effect, leading to different spectral shapes between absorption and Raman spectra.^{102,103} The cumulant expansion assumes the adiabatic approximation, where eigenstates do not significantly mix and can, thus, be followed in time. The second-order cumulant expression for different spectroscopic techniques can be found in the literature.^{69,100,104–108}

The NISE approach is based on explicitly solving the time-dependent Schrödinger equation by dividing time into small intervals, during which the Hamiltonian can be considered constant, and then successively solving the quantum dynamics for subsequent time intervals. For one such interval, the solution to the time-dependent Schrödinger equation is given by

$$\phi(t + \Delta t) = U(t + \Delta t, t)\phi(t) = \exp\left(-\frac{i}{\hbar}H(t)\Delta t\right)\phi(t). \quad (11)$$

Here, $\phi(t)$ is the wave function at time t , $U(t + \Delta t)$ is the time-evolution operator from time t to time $t + \Delta t$, and $H(t)$ is the fixed Hamiltonian at time t along a trajectory as defined by Eq. (1). In this approach, the time-evolution operator for an arbitrary number of consecutive time steps can be found through a time-ordered product,

$$U(t + n\Delta t, t) = \prod_{j=1}^n U(t + j\Delta t, t + (j-1)\Delta t). \quad (12)$$

The superscript ' on the product shows that the matrix product should be performed in a time-ordered manner. In the NISE approach, the absorption spectrum is given by

$$I(\omega) = \int_0^\infty dt \sum_{\alpha=x,y,z} \langle \langle g | \mu_\alpha(t + t_0) U(t + t_0, t_0) \mu_\alpha(t_0) | g \rangle \rangle \exp(-i\omega t). \quad (13)$$

Here, the outer brackets denote the ensemble average over different starting points (t_0) along the Hamiltonian trajectory, and the subscript α on the transition dipole shows the Cartesian component of the vector. $|g\rangle$ denotes the ground state of the system. The averaging over transition dipoles and over the time evolution is performed explicitly along the trajectory. This has the advantage that the non-Condon, non-Gaussian, and non-adiabatic effects are accounted for.⁸⁶ The weakness of this approach is that it neglects the effect of the system on the bath and, therefore, does not thermalize correctly and formally corresponding to an infinite temperature approximation. In practice, this is not a significant problem as long as the bandwidth of the simulated spectrum is narrow compared to the thermal energy or as long as the dynamics considered is fast compared to the time scale of thermalization.¹⁰⁹ A generalization to include the feedback of the system on the bath using a surface-hopping type scheme has been considered.^{110,111} In the NISE approach, the inclusion of relaxation back to the ground state is also neglected. This relaxation is often accounted for by simply assuming an overall exponential decay. Describing this relaxation properly requires models explicitly including, for example, intermediate states and allows the energy flow between the classical bath and the quantum system. Such treatment is possible with other methods.^{112,113}

The HEOM approach⁹⁶ is based on simultaneously describing the system and the bath including correlations between the two. This can be done exactly when the bath is a collection of independent

harmonic oscillators and the system–bath coupling is linear. The bath is, thus, approximated by spectral density. The system dynamics is described by a reduced density operator ρ and a hierarchy of auxiliary operators that take the fluctuation of the electronic energy and dissipation of reorganization energy into account. Formally, the hierarchy is infinite, but, in practice, it can be truncated at a level depending on the strength of the system–bath coupling. In essence, the larger the reorganization energy [see Eq. (6)], the deeper one needs to go in the hierarchy for convergence. The equations to determine the system density matrix are too extensive to summarize in detail here. A clear description of the procedure is provided in Ref. 95. The absorption spectrum can then be obtained from

$$I(\omega) = \int_0^\infty dt \sum_{\alpha=x,y,z} \text{Tr}(\mu_\alpha \tilde{U}(t,0) \mu_\alpha \rho(0)) \exp(-i\omega t). \quad (14)$$

Here, $\tilde{U}(t,0)$ is the Liouville space time-evolution operator for the full hierarchy and $\rho(0)$ is the ground state density matrix. In the HEOM approach, the Condon and Gaussian approximations are made. The advantage compared to the second-order cumulant expansion is that non-adiabatic effects are accounted for. A number of implementations for HEOM calculations have been published,^{79,114–118} and numerous applications to spectroscopic problems have been presented.^{118–124}

Other approaches exist for calculating spectra in similar ways to the approach discussed here in detail. These, for example, include the Redfield approach,¹²⁵ path-integral methods,¹²⁶ and various classical and semi-classical approximations.^{127–132}

H. Spectra

Above, I focused on the calculation of the absorption spectra. These are typically the first to calculate and a good initial test for the validity of the spectral model. The absorption spectra of complex structures are often surprisingly simple and dominated by a few bright states that carry all the oscillator strength. For example, for linear aggregates, one dominant state is observed either at the top (H-aggregate) or at the bottom (J-aggregate) of the band of eigenstates, resulting in a blue- or red-shift of the spectrum compared to the monomer spectrum. The shift is determined by the angle between the transition dipoles of the individual molecules and the axis of the linear aggregate. If the transition-dipole coupling model describes the interactions correctly, a blue-shift is expected for angles larger than the so-called magic angle (54.7°) and a red-shift for smaller angles.^{133–135} For two-dimensional films, more complex rules apply.¹³⁶ In circular or tubular structures, two dominant peaks arise. One peak corresponds to eigenstates with the transition dipole parallel to the tube axis, while the other peak corresponds to eigenstates with the transition dipole perpendicular to the tube axis.^{137,138} The relative intensity of the two peaks can be used to determine the angle,^{138,139} β , between the transition dipole of the dye molecules and the tubular axis using $\tan(\beta) = \sqrt{\frac{2f_{\perp}}{f_{\parallel}}}$. In similar ways, other more complex structures give rise to spectral signatures in the absorption spectra, which are largely determined by the symmetry.

In linear dichroism spectra,¹⁴⁰ the difference between the absorption parallel to one axis and the absorption perpendicular to that axis is measured for a sample, where the intrinsic structures are

aligned. Often, the linear dichroism spectrum is then further normalized with respect to the absorption spectrum. This allows for a more explicit separation of peaks with different symmetries as discussed above. The β angle for a tubular aggregate is, thus, determined more accurately with the assistance of linear dichroism. In practice, the alignment of the supermolecular structures is not perfect, resulting in an uncertainty in the determined angle comparable to the uncertainty in the alignment.

Circular dichroism (CD) is defined as the difference in absorption of left and right polarized light. A circular dichroism signal requires a chiral sample, and the spectra are sensitive to the helicity of the structure. The spectra are generally challenging to model and contain three different contributions. Each individual molecule may be chiral and contributes to the CD spectrum. The overall chirality of the eigenstates resulting from the chirality of the underlying structure will result in a chiral signal. Furthermore, in anisotropic samples, an overall anisotropic chiral signal can arise.¹⁴¹ In essence, the CD spectra depend on the chirality of the exciton states, which is very sensitive to the degree of delocalization of the states.^{142–144} CD spectroscopy may, thus, provide a very sensitive probe of delocalization.

Non-linear spectroscopic techniques provide a window to more sensitive structural determination and sensitivity to structural dynamics. The most prominent methods in this respect are two-dimensional spectroscopies.^{32,33,145–147} The power of these techniques is that the two-dimensional spectra exhibit cross-peaks between coupled states. Using experiments with laser light with different polarization, the relative orientation between the transition dipoles of the states can be determined.^{100,148,149} Furthermore, these techniques provide a window to follow structural dynamics in real time as the delay between pump pulses and probe pulses can be varied.¹⁵⁰ A wide range of other non-linear spectroscopic techniques is available providing insight into different sample properties.^{7,14,151–161} A significant effort has been invested in the efficient calculation of two-dimensional spectroscopic signals.^{46,89,162,163}

I. Test against experiment

It is a crucial step to compare the simulated models against experiment. Unless theory and experiment reasonably agree, there is a discrepancy in one of the steps involved. It is desirable to test the model for simple systems such as isolated molecules in different solvents.^{62,86,164} Furthermore, tests can be made for multiple well-known structures,^{67,165–169} providing confidence that the elements used in the computational modeling are all reliable. When comparing with experiment, it is crucial to remember that the matching simulated conditions and experimental conditions are often very challenging and sometimes even impossible. For example, infrared spectra of the amide I region of proteins are often performed in heavy water to eliminate the spectral contribution from the water bend. This also leads to an exchange of the acidic protons including those in the backbone. The time needed to exchange all protons depends on the complexity of the protein structure,^{170,171} and some protons may not exchange at all, which is difficult to account for in modeling. In biological samples, the details of the lipid composition around membrane proteins may be unknown. The state of a sample due to handling conditions may influence spectra, and impurities

and defects can contribute to spectra. Furthermore, simulations are often biased toward starting structures, and true experimental inhomogeneities may be challenging to capture.¹¹¹ The finite pulse and intensity effect in experiments may further complicate the comparison.¹⁷² A careful evaluation of the observed differences is, therefore, important before interpretation of spectra. Depending on the outcome of the test against experiment, one may also decide to refine the model or simulation method.

J. Force field refinement

In some cases, discrepancy between simulation and experiment may indicate that an adjustment of the force field used for the molecular dynamics simulations is needed. Hydrogen bonding is, for example, often reflected in the observed spectra, and incorrect population of different hydrogen bonding states^{62,84,173–176} may help guide a force field improvement^{177–181} or choice of the force field. Comparing spectra for different force fields is wise when attacking new problems.^{168,169,175,182,183} The force field charges affect the Hamiltonian, and the structure often depends quite sensitively on the force field.¹⁸⁴

K. Structure refinement

Computational spectroscopy can be used to determine the structure of systems by comparing spectra of candidate structures with experimentally observed spectra. Comparing simulated 2DIR spectra with experimental observations, for example, allowed probing the gating mechanism of the M2 channel of the influenza virus,^{185,186} the hydrogen bond structure in elastin such as peptides,^{187,188} the structural change in redox active proteins,¹⁸⁹ and the gating mechanism in Refs. 190–192. Comparing absorption and linear dichroism spectra of natural light-harvesting chlorosomes allowed determining the global rolling angle in these structures,^{139,193} with single aggregate measurements even providing insight into variation between individual chlorosomes. Furthermore, analysis of the spectral variation in single walled tubular aggregates mimicking the chlorosome of the local angular variation in the packing could be determined by comparing computational spectra and single aggregate spectra.¹⁹⁴ Combining molecular dynamics, quantum chemistry, and spectral modeling, the spectra of double-walled tubular aggregates formed by cyanine dyes were simulated and used for refining the local molecular packing of the cyanine dyes.^{64,195}

L. Analysis, prediction, and interpretation

When the desired agreement between simulated spectra and experimental data is obtained, interpretation can be made based on different types of analysis, and predictions can be made of other spectral signals, which may help reveal new properties. A few examples of useful properties to analyze are given below.

The exciton delocalization reveals how many chromophores are involved in a given eigenstate or a collection of eigenstates. Different measures exist for this, where the most commonly used is possibly the participation number or participation ratio: $P_m = \frac{1}{\sum_n |c_{nm}|^4}$.¹⁹⁶ The definition here is given for a specific eigenstate m , where the wave function coefficients for each chromophore are c_{nm} ; however, often this quantity is averaged over many eigenstates,

for example, for the complete exciton band or for the optically active states.^{197–199} Another useful measure of the delocalization is the spatial correlation function:^{199–201} $C(\vec{r}) = \langle \sum_{n,l} \sum_m c_{nm} c_{lm}^* \delta(\vec{r}_{nl} - \vec{r}) \rangle / \langle \sum_{n,l} \delta(\vec{r}_{nl} - \vec{r}) \rangle$, where the distance between pairs of chromophores, \vec{r}_{nl} , can be calculated on a grid, when a regular crystal structure is used. Restrictions can be imposed on the sum over the eigenstates, m , to learn about differences between states in different spectral regions.

Different kinds of structural correlation functions may provide useful insights. This can range from the Debye–Waller factor also known from x-ray diffraction, which reveals information about local flexibility.²⁰² The radial distribution function, which is also related to the structure factor,²⁰³ provides information about the local structural order. A joint radial–angular distribution function,²⁰⁴ $g(r, \Theta) = \langle \sum_{n,l} \delta(r_{nl} - r) \delta(\Theta_{nl} - \Theta) \rangle$, where r_{nl} is the distance between the dye molecules and Θ_{nl} is the angle between their transition-dipole moments, may provide useful insight as the exciton couplings depend both on local distances and angles between transition dipoles. An increase in local order was found to be correlated with a reduction in the sum of the signed coupling between an individual dye molecule and all other dye molecules.⁶⁴ For simple linear aggregates, this quantity measuring the coupling strength is related to the shift in the absorption peak of the full system compared to the absorption of the isolated dye molecule.¹³³

Pump–probe and two-dimensional spectroscopies using a different polarization of the pump and probe pulses are sensitive to reorientational motion.^{205–208} For individual chromophores, the time evolution of the resulting anisotropic signal is determined by the orientational correlation function $r(t) = \frac{1}{5}(3 \cos^2(\Theta(t)) - 1)$, where $\Theta(t)$ is the angle between the transition-dipole moment of the individual molecule at different times. Furthermore, two-dimensional spectroscopies allow the determination of the angle between transition dipoles of different eigenstates by examining the intensity of the resulting cross-peaks.^{148,209,210}

For coupled systems, exciton dynamics may lead to an additional decay of the anisotropy.^{31,46,211,212} Such population dynamics can be analyzed through the population transfer between different sites $P_{nl}(t) = \langle U_{nl}(t, 0) \rangle$, where analysis of different initial, l , and final states, n , can provide useful insight. The nature of the population transfer in biological systems has been debated,^{213,214} and analysis of the population dynamics in photosynthetic systems has been widely studied computationally.^{34,95,111,215–219}

Predictions of improved experimental setups and design of improved materials may be obtained based on the analysis and understanding gained from the computational spectroscopy.

III. EXAMPLE FOR VIBRATIONAL SPECTROSCOPY

Computational spectroscopy has been applied with quite a lot of success to describe vibrational spectroscopy. The amide I band of proteins is an application of special interest^{32,220,221} due to the great structural variation in proteins and the sensitivity of the amide I band to the structure. The amide I vibrations are dominated by the CO-stretch vibration in the peptide unit, which is present in every amino acid in the protein backbone and in certain side chains. The transition dipole of this vibration is quite large, resulting in

large couplings, delocalization of the vibrations, and structural sensitivity. The α -helix,²²² 3^{10} -helix,²²³ and β -sheet²²⁴ secondary structural motifs have attracted special attention due to their abundance. As an illustration of the application to vibrational spectroscopy, the amide I spectra of a snowflea anti-freeze protein were calculated. This protein is dominated by the polyproline-II helix²²⁵ secondary structure motif (see Fig. 3). For this, the 2pne protein database structure²²⁶ was used. Nine sodium ions and ten chlorine ions were added to keep the simulation box neutral and a realistic ionic strength. Molecular dynamics simulations were performed with the OPLS-AA force field⁴⁰ using 2 fs time steps, the Verlet algorithm²²⁷ for solving the dynamics, and the particle mesh Ewald method for accounting long range electrostatic interactions.²²⁸ After a 1 ns equilibration run using the V-rescale²²⁹ and Parrinello–Rahman²³⁰ algorithms for keeping temperature and pressure constant, a 1 ns NPT production run was made with the configurations stored every 20 fs for input for the spectral simulations. The simulations were performed in the GROMACS simulation package²³¹ version 5.1.2.

The amide I Hamiltonian was extracted from the MD trajectories with the AmideImaps utility.²³⁴ The amide I vibrational frequencies were predicted using a transferable electrostatic map⁶² using a 20 Å cutoff for the electrostatic interactions, including a nearest neighbor correction.²³⁵ A transition charge coupling map²³⁵ was used to predict the long range couplings, while a nearest neighbor map²³⁵ was used for couplings between adjacent residues. For pre-proline units, adapted mappings were used.²³⁶ In the present simulations, side chain vibrations were neglected. The anharmonicity used for the two-dimensional infrared simulations was set to 16 cm⁻¹.³²

Spectra were calculated using the NISE_2017 code.⁹⁰ The coherence times were varied from 0 to 5.12 ps for all considered spectroscopic techniques. A 1 ps exponential apodization function was applied for both coherence times for smoothening. 1000 disorder realizations sampled equidistantly along the Hamiltonian trajectory were used for the absorption and vibrational circular dichroism (VCD), while 100 disorder realizations were used for the two-dimensional infrared spectra. The calculated absorption, VCD,

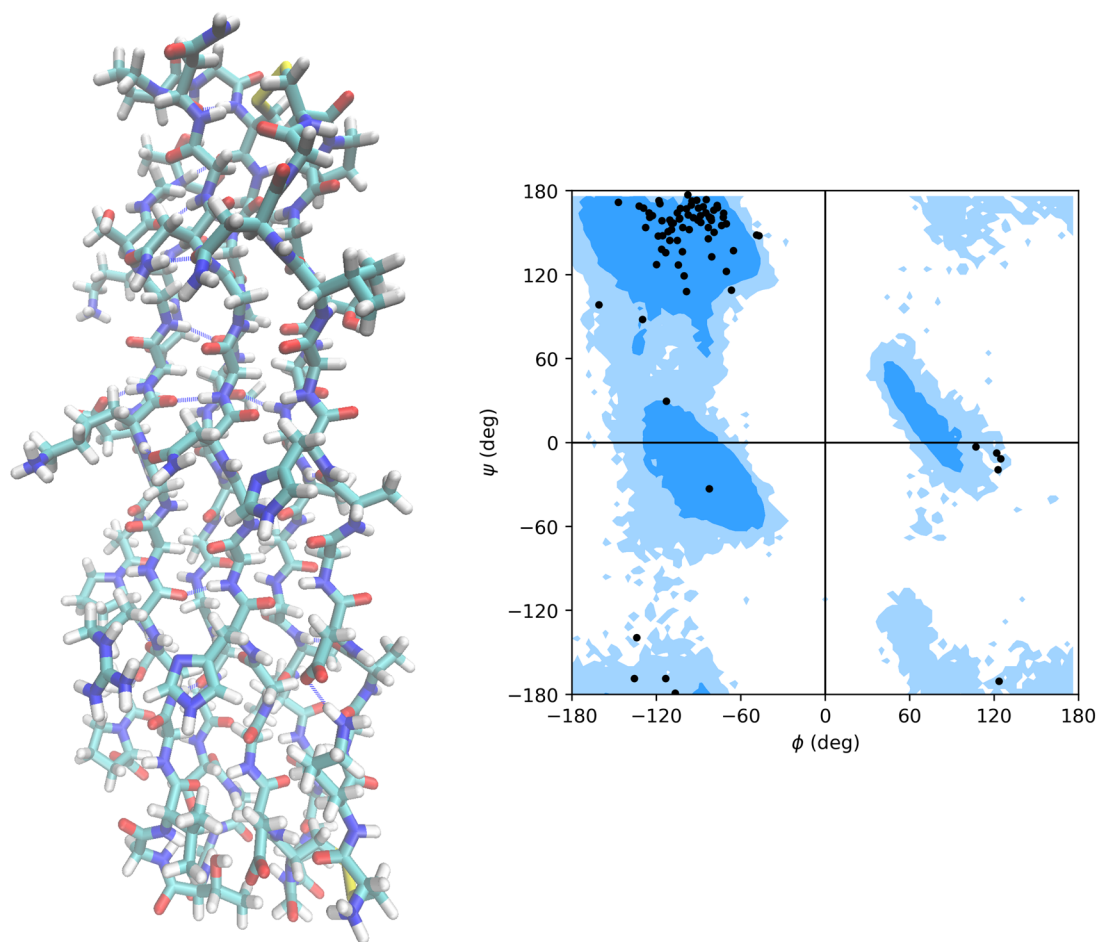


FIG. 3. The 2pne structure of the snowflea anti-freeze protein (left) and the corresponding Ramachandran angle²³² plot generated with MD analysis (right).²³³ The blue contours indicate the most common Ramachandran angles.

and two-dimensional infrared spectra of the snowflea anti-freeze protein are shown in Fig. 4. The higher spectral sensitivity of the VCD calculated and two-dimensional infrared spectra are clear. While four overlapping spectral bands can be identified in the absorption spectrum, the VCD spectrum clearly exhibits two negative features (at 1625 and 1690 cm^{-1}) and two positive features (at 1652 and 1676 cm^{-1}). The bands observed in the two-dimensional infrared spectra also reveal more spectral features than the absorption spectrum, and detailed analysis of the relative

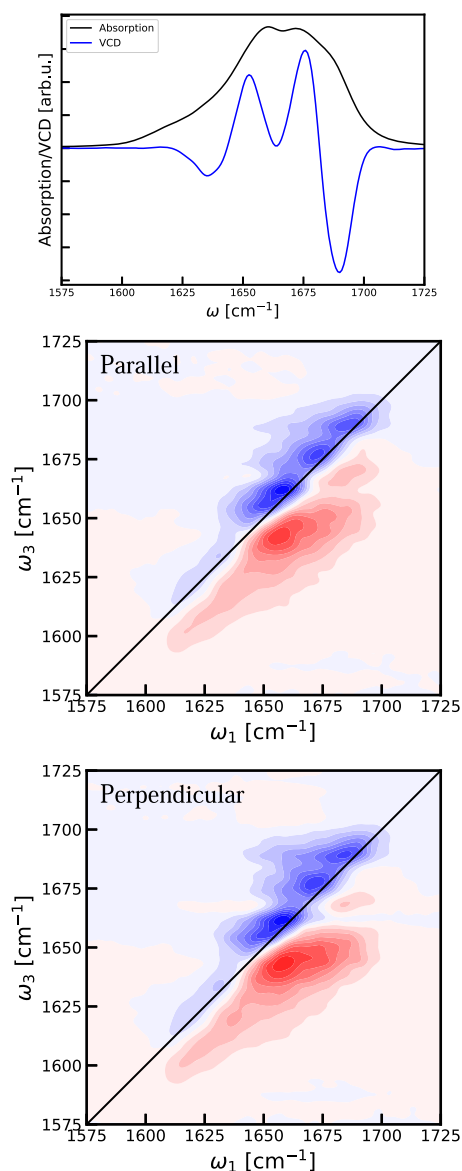


FIG. 4. The linear absorption and vibrational circular dichroism calculated for the amide I spectral region is shown at the top. Below are the two-dimensional infrared spectra calculated for zero waiting time with parallel and perpendicular laser polarizations, respectively. Equidistant contours are drawn for every 10% of the maximal signal. Blue contours are drawn for bleach/stimulated emission, and red contours are used for the excited state absorption signal.

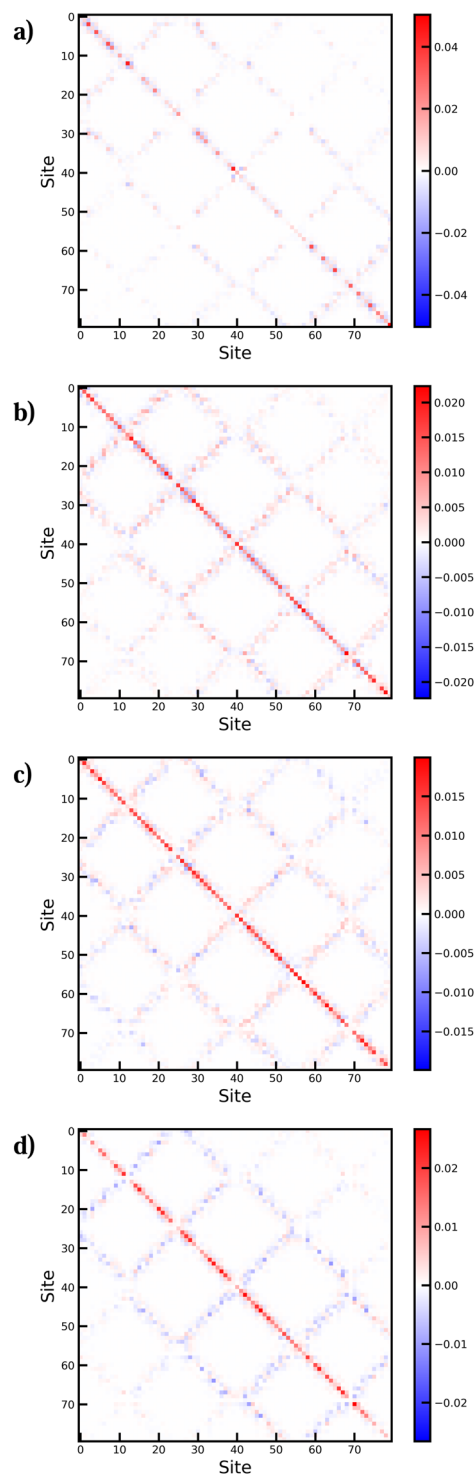


FIG. 5. The density matrices averaged over the amide I eigenstates along the Hamiltonian trajectory for the snowflea anti-freeze protein in 10 cm^{-1} wide bins centered around the peak positions: (a) 1636 cm^{-1} , (b) 1660 cm^{-1} , (c) 1673 cm^{-1} , and (d) 1690 cm^{-1} . The site numbers start at 0 for the N-terminal amide I running to 79 for the C-terminal amide I. Off-diagonal elements (coherences) illustrate the in-phase motion of the CO bonds (red) and out-of-phase motion (blue).

peak intensities can be used to elucidate more structural information. Isotope labeling can potentially be used to reveal site-specific information.^{237,238}

The nature of the different transitions was elucidated with the density matrix calculated for all eigenstates along the Hamiltonian trajectory in 10 cm⁻¹ wide bins centered at the four main peaks (Fig. 5). The density matrix elements in the site basis are

$$\rho_{kl}(\omega_{\min}, \omega_{\max}) = \left\langle \sum_j c_{jk} c_{jl}^* \Pi(\omega_j, \omega_{\min}, \omega_{\max}) \right\rangle, \quad (15)$$

where the frequencies ω_{\min} and ω_{\max} define the relevant frequency window, and c_{jk} and c_{jl}^* are the wave function coefficients for eigenstate j . The function $\Pi(\omega_j, \omega_{\min}, \omega_{\max})$ is zero when the frequency (ω_j) of eigenstate j is outside the specified frequency window and one inside. The brackets denote averaging over the full Hamiltonian trajectory. The tail at 1617 cm⁻¹ is localized at pre-proline residues, which typically have a frequency about 25 cm⁻¹ below the main band,²³⁶ and the density matrix is not shown here. The states behind the main peaks are delocalized both along the backbone and over neighboring polyproline-II helix strands. The picture is very similar to that seen in β -sheets,^{224,239} however, it contains both parallel and anti-parallel neighbors as seen by the presence of both diagonal and anti-diagonal coherence lines in the density matrices. The four transitions can, therefore, be assigned in a way very similar to that of β -sheet transitions. For the transitions at 1636 and 1660 cm⁻¹, the wave functions between nearest neighbors along the backbone are anti-correlated as seen by the blue color at the first sub-diagonals of the density matrices. In other words, when one CO bond in the backbone stretches, then the nearest neighbor CO bonds contract. The transitions at 1673 and 1690 cm⁻¹ are positively correlated between nearest neighbors along the backbone. For the transitions at 1636 and 1690 cm⁻¹, the vibrations on neighboring strands are predominantly out-of-phase, while the vibrations on neighboring strands are predominantly in-phase for the transitions at 1660 and 1673 cm⁻¹. The spectra of polyproline-II helices, thus, have quite some similarity to the spectra of β -sheets; however, the selection rules are different due to the three-dimensional structure of the helices, and where the lowest frequency peak is dominant in β -sheets, the peak has the lowest intensity in the polyproline-II helix structure (Fig. 5).

IV. EXAMPLE FOR ELECTRONIC SPECTROSCOPY

Computational spectroscopy of the natural light-harvesting systems is crucial for both understanding the local structure and the dynamics of excitons from the site of initial excitation to the reaction center, where the electronic energy is converted into chemical energy. In the following, examples of spectra of the LH2 complex of purple bacteria are provided. A number of these spectra were already provided in Ref. 31, where a detailed description of the simulation parameters is also provided. In short, the couplings between different bacteriochlorophyll a molecules were determined using the 1kzu protein databank structure²⁴⁰ using the transition-dipole coupling model. The bath dynamics was modeled with a single overdamped Brownian oscillator [see Eq. (6)] for each molecule with the parameters adjusted to reproduce the linear absorption spectra.³¹ The used structure is shown in Fig. 6 next to the simulated

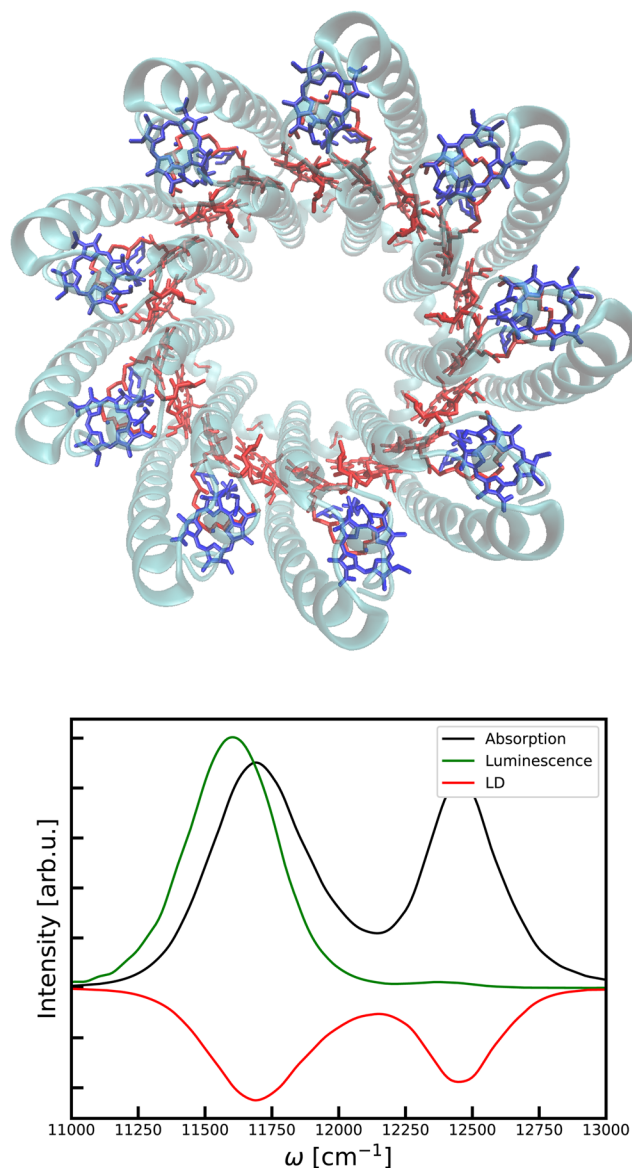


FIG. 6. (Top) Illustration of the structure of the *Rhodospseudomonas acidophila*. The protein scaffold is illustrated in cyan. The B850 bacteriochlorophylls are shown in red, and the B800 bacteriochlorophylls are shown in blue. (Bottom) Linear spectra calculated for the LH2 system. The model used was previously described in Ref. 31.

linear absorption, linear dichroism, and fluorescence spectra. These spectra were all obtained using the NISE simulation program and protocol discussed above. The fluorescence spectrum was obtained by introducing a Boltzmann weighting factor for each eigenstate in Eq. (14) to account for the thermal relaxation on the excited state before emission.

The linear spectra show two main peaks, one at 11 500 cm⁻¹ (850 nm) and one at 12 500 cm⁻¹ (800 nm), and compare well with experimental observations,²⁴¹ and their origin has been discussed in

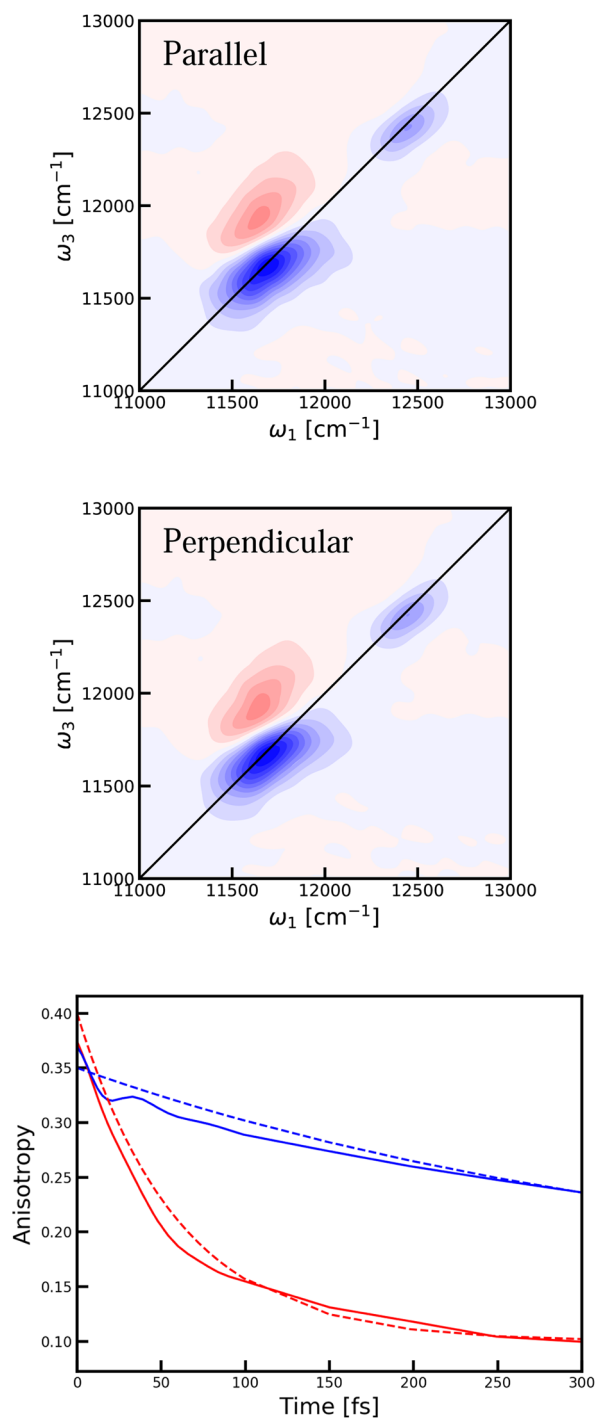


FIG. 7. (Top) Two-dimensional electronic spectrum of LH2 with parallel polarization at zero waiting time. (Middle) Two-dimensional electronic spectrum of LH2 with perpendicular polarization at zero waiting time. Equidistant contours are drawn for every 10% of the maximal signal. Blue contours are drawn for bleach/stimulated emission, and red contours are used for the excited state absorption signal. (Bottom) Polarization anisotropy as a function of waiting time obtained at the B850 (red) and B800 (blue) diagonal positions of the two-dimensional electronic spectra. Experimental data from Ref. 212 are shown with dashed lines.

numerous theory papers.^{242,243} The first peak arises from the closely packed chromophores, as shown in red in the structure, while the second peak arises from the less strongly interacting chromophores, illustrated in blue. The linear dichroism spectrum is negative for both peaks, revealing that the transition-dipole moments of the chromophores have the largest component in the x, y -plane, which is the plane perpendicular to the ring axis. The fluorescence spectrum exhibits one red-shifted peak as the emission happens from the lowest energy states. Emission from the B800 chromophores is heavily suppressed, and even in the B850 band, the emission is enhanced for the low energy states. From previous theory studies, it is well-known that the low-frequency peak is dominated by the so-called $k = \pm 1$ exciton states,²⁴⁴ which are delocalized over three to eight bacteriochlorophyll molecules.^{109,245}

The calculated two-dimensional electronic spectra are presented for both the parallel and perpendicular laser polarization configurations shown in Fig. 7. The time delay between the excitation and detection pulses in the plotted spectra was set to zero. Both spectra exhibit peaks on the diagonal at the same positions, where peaks are observed in the linear absorption. These peaks contain ground state bleach and stimulated emission contributions from the two types of chromophores. Above the peak at $11\,500\text{ cm}^{-1}$ (850 nm), an absorptive feature is observed. This arises as absorption of the single excited states to higher excited states becomes possible as the coupling between the involved chromophores is large enough to result in significant delocalization of the single excited states over the ring of chromophores. In experimental spectra,^{212,246,247} these features are also clearly visible. The results are also in good agreement with other simulations.^{109,248} From further simulations with longer time delays, one can extract the anisotropy for the two diagonal peaks. This is shown in Fig. 7 together with the experimental anisotropy extracted from Ref. 212. The dye molecules inside the protein do not reorient, and the motion of individual chromophores, thus, cannot explain the anisotropy decay. The explanation of the decay is that due to the coupling between chromophores, the excitations move on the chromophore rings, and as the different chromophores have different directions of their transition dipoles, the effective transition dipole for any excited state is scrambled in the x, y -plane. The faster anisotropy decay in the B850 band is a reflection of the stronger coupling between these closely stacked chromophores.

A set of tutorial files including all the inputs used for the LH2 example can be found on GitHub.²⁴⁹

V. CONCLUDING DISCUSSION AND FUTURE DIRECTIONS

In this Perspective, I provided an overview of different aspects of computational spectroscopy on complex systems and an overview of different approaches that may be applied to build a bridge between structural modeling and experimental spectroscopy. While computational spectroscopy has celebrated many successes, the continuous developments in experimental setups and computational science lead to new challenges and opportunities. In the following, some of these will be discussed.

The prediction of molecular excitation energies with frequency mappings has been a great success.⁵⁵ However, with recent developments in the application of machine learning to chemical

problems,^{250,251} extension to improving, for example, the prediction of excitation energies needed in computational spectroscopy applications is a new development.^{252–256} In some sense, this development is merely an extension of the linear regression used in the mapping approaches. A machine learning approach has also been used to directly predict unknown parameters to model two-dimensional spectroscopic data.²⁵⁷ For future machine learning improvements, important challenges are to keep the high calculation efficiency of the mapping approaches and the ease of interpretation while still improving the accuracy of the modeling of two-dimensional spectroscopic data. If machine learning is merely implemented to allow blackbox spectral calculations, *one will observe machine learning without human learning and, therefore, no scientific progress.*

The development of new computational architectures provides new opportunities for efficient implementations of computational spectroscopic methods. Examples of implementations for large scale calculations include parallel computing using the Message Passing Interface (MPI),³¹ the Open Multi-Processing (OpenMP),^{89,115} and Graphical Processing Unit (GPU)^{114,258,259} implementations. The use of quantum computing for such applications is still in its infancy,²⁶⁰ but with rapid developments in quantum technology,²⁶¹ such hardware will provide powerful computational spectroscopy.

Computational spectroscopy may approach a new multiscale era compared to the development seen in molecular dynamics with the introduction of coarse grained modeling.^{262,263} Computational spectroscopy has already been performed using the input from coarse grained molecular dynamics,^{35,264} following a backmapping procedure⁴³ to retrieve atomistic information. However, an extension of the multiscale approach to make the spectroscopic calculation span multiple lengths and/or time scales is a new challenge. A few promising steps in this direction include the development of efficient methods for predicting the dynamics of excited states in extensive systems such as the kinetic network model,^{265–267} DM-HEOM,²¹⁹ and multi-chromophoric Förster energy transfer models.^{76,268} Combining such approaches to calculate time-resolved spectra for large complex systems will be an important new direction.

Recent development of broad band spectrometers^{269–271} and spectroscopies combining very different spectral regions^{160,272,273} provides new opportunities to probe interactions between states with very different energies and to simultaneously probe dynamics over broad spectral ranges. At the same time, this poses new challenges to the computational approaches to include the relevant states at an equal level of theory. This again may require a multiscale approach to treat the broad scale of energies needed, and so far, theoretical approaches have been limited to small systems, typically involving a single molecule.^{160,272,274–277}

Action spectroscopies are another avenue of spectroscopic methods, which are often hard to predict and model at the microscopic level. Spectroscopies that use a charge current,^{154,161} a photoemission electron,¹⁵³ or a fluorescence^{7,161,278} readout may provide very powerful functional information. However, modeling the details of the processes behind the action responsible for the readout is often far from straightforward. Such spectroscopies, thus, pose future exciting challenges for the field of computational spectroscopy. The development of explicit and approximate ways of simulating the new detection schemes is, therefore, crucial.

AUTHOR DECLARATIONS

Conflict of Interest

The authors have no conflicts to disclose.

DATA AVAILABILITY

The data that support the findings of this study are available from the corresponding author upon reasonable request.

REFERENCES

- ¹O. Guvench and C. L. Brooks, *J. Am. Chem. Soc.* **127**, 4668 (2005).
- ²D.-L. Long, E. Burkholder, and L. Cronin, *Chem. Soc. Rev.* **36**, 105 (2007).
- ³B. Kriete, A. S. Bondarenko, V. R. Jumde, L. E. Franken, A. J. Minnaard, T. L. C. Jansen, J. Knoester, and M. S. Pshenichnikov, *J. Phys. Chem. Lett.* **8**, 2895 (2017).
- ⁴A. Majumdar and T. L. C. Jansen, *J. Phys. Chem. Lett.* **12**, 5512 (2021).
- ⁵M. Aeschlimann, T. Brixner, A. Fischer, C. Kramer, P. Melchior, W. Pfeiffer, C. Schneider, C. Strüber, P. Tuchscherer, and D. V. Voronine, *Science* **333**, 1723 (2011).
- ⁶C. R. Baiz, D. Schach, and A. Tokmakoff, *Opt. Express* **22**, 18724 (2014).
- ⁷V. Tiwari, Y. A. Matutes, A. T. Gardiner, T. L. C. Jansen, R. J. Cogdell, and J. P. Ogilvie, *Nat. Commun.* **9**, 4219 (2018).
- ⁸K. M. Tracy, M. V. Barich, C. L. Carver, B. M. Luther, and A. T. Krummel, *J. Phys. Chem. Lett.* **7**, 4865 (2016).
- ⁹P. Hamm, *J. Chem. Phys.* **154**, 104201 (2021).
- ¹⁰D. Lotti, P. Hamm, and J. P. Kraack, *J. Phys. Chem. C* **120**, 2883 (2016).
- ¹¹A. M. Alperstein, J. S. Ostrander, T. O. Zhang, and M. T. Zanni, *Proc. Natl. Acad. Sci. U. S. A.* **116**, 6602 (2019).
- ¹²H. Graener and G. Seifert, *Chem. Phys. Lett.* **185**, 68 (1991).
- ¹³L. W. Barbour, M. Hegadorn, and J. B. Asbury, *J. Phys. Chem. B* **110**, 24281 (2006).
- ¹⁴A. Shalit, S. Ahmed, J. Savolainen, and P. Hamm, *Nat. Chem.* **9**, 273 (2016).
- ¹⁵E. V. Kahl, J. C. Berengut, M. Laatiaoui, E. Eliav, and A. Borschevsky, *Phys. Rev. A* **100**, 062505 (2019).
- ¹⁶A. Cembran, R. González-Luque, P. Altoè, M. Merchán, F. Bernardi, M. Olivucci, and M. Garavelli, *J. Phys. Chem. A* **109**, 6597 (2005).
- ¹⁷A. Klamt and G. Schüürmann, *J. Chem. Soc., Perkin Trans. 2* **1993**, 799.
- ¹⁸Y. Takano and K. N. Houk, *J. Chem. Theory Comput.* **1**, 70 (2004).
- ¹⁹A. Pedone, M. Biczysko, and V. Barone, *ChemPhysChem* **11**, 1812 (2010).
- ²⁰V. Barone, I. Carnimeo, and G. Scalmani, *J. Chem. Theory Comput.* **9**, 2052 (2013).
- ²¹C. Puzzarini, J. Bloino, N. Tasinato, and V. Barone, *Chem. Rev.* **119**, 8131 (2019).
- ²²G. D. Scholes, C. Curutchet, B. Mennucci, R. Cammi, and J. Tomasi, *J. Phys. Chem. B* **111**, 6978 (2007).
- ²³C. König and J. Neugebauer, *J. Chem. Theory Comput.* **9**, 1808 (2013).
- ²⁴L. Jensen, P.-O. Åstrand, A. Osted, J. Kongsted, and K. V. Mikkelsen, *J. Chem. Phys.* **116**, 4001 (2002).
- ²⁵O. Weingart, A. Nenov, P. Altoè, I. Rivalta, J. Segarra-Martí, I. Dokukina, and M. Garavelli, *J. Mol. Model.* **24**, 271 (2018).
- ²⁶J. Adolphs, F. Müh, M. E.-A. Madjet, and T. Renger, *Photosynth. Res.* **95**, 197 (2008).
- ²⁷S. Ham and M. Cho, *J. Chem. Phys.* **118**, 6915 (2003).
- ²⁸T. Renger and F. Müh, *Photosynth. Res.* **111**, 47 (2012).
- ²⁹P. Hamm and S. Woutersen, *Bull. Chem. Soc. Jpn.* **75**, 985 (2002).
- ³⁰F. Segatta, A. Nenov, D. R. Nascimento, N. Govind, S. Mukamel, and M. Garavelli, *J. Comput. Chem.* **42**, 644 (2021).
- ³¹A. S. Sardjan, F. P. Westerman, J. P. Ogilvie, and T. L. C. Jansen, *J. Phys. Chem. B* **124**, 9420 (2020).
- ³²P. Hamm, M. Lim, and R. M. Hochstrasser, *J. Phys. Chem. B* **102**, 6123 (1998).
- ³³J. D. Hybl, A. W. Albrecht, S. M. Gallagher Faeder, and D. M. Jonas, *Chem. Phys. Lett.* **297**, 307 (1998).

- ³⁴C. Olbrich, T. L. C. Jansen, J. Liebers, M. Aghtar, J. Strümpfer, K. Schulten, J. Knoester, and U. Kleinekathöfer, *J. Phys. Chem. B* **115**, 8609 (2011).
- ³⁵C. Liang, M. Louhivuori, S. J. Marrink, T. L. C. Jansen, and J. Knoester, *J. Phys. Chem. Lett.* **4**, 448 (2013).
- ³⁶S. K. Burley, H. M. Berman, C. Bhikadiya, C. Bi, L. Chen, L. Di Costanzo, C. Christie, K. Dalenberg, J. M. Duarte, S. Dutta, Z. Feng, S. Ghosh, D. S. Goodsell, R. K. Green, V. Guranović, D. Guzenko, B. P. Hudson, T. Kalro, Y. Liang, R. Lowe, H. Namkoong, E. Peisach, I. Periskova, A. Prlić, C. Randle, A. Rose, P. Rose, R. Sala, M. Sekharan, C. Shao, L. Tan, Y.-P. Tao, Y. Valasatava, M. Voigt, J. Westbrook, J. Woo, H. Yang, J. Young, M. Zhuravleva, and C. Zardecki, *Nucleic Acids Res.* **47**, D464 (2018).
- ³⁷J. Jumper, R. Evans, A. Pritzel, T. Green, M. Figurnov, O. Ronneberger, K. Tunyasuvunakool, R. Bates, A. Židek, A. Potapenko, A. Bridgland, C. Meyer, S. A. A. Kohl, A. J. Ballard, A. Cowie, B. Romera-Paredes, S. Nikolov, R. Jain, J. Adler, T. Back, S. Petersen, D. Reiman, E. Clancy, M. Zielinski, M. Steinegger, M. Pacholska, T. Berghammer, S. Bodenstein, D. Silver, O. Vinyals, A. W. Senior, K. Kavukcuoglu, P. Kohli, and D. Hassabis, *Nature* **596**, 583 (2021).
- ³⁸W. L. Jorgensen, J. Chandrasekhar, J. D. Madura, R. W. Impey, and M. L. Klein, *J. Chem. Phys.* **79**, 926 (1983).
- ³⁹H. J. C. Berendsen, J. R. Grigera, and T. P. Straatsma, *J. Phys. Chem.* **91**, 6269 (1987).
- ⁴⁰W. L. Jorgensen and P. Schyman, *J. Chem. Theory Comput.* **8**, 3895 (2012).
- ⁴¹K. Lindorff-Larsen, S. Piana, K. Palmo, P. Maragakis, J. L. Klepeis, R. O. Dror, and D. E. Shaw, *Proteins* **78**, 1950 (2010).
- ⁴²C. Oostenbrink, T. A. Soares, N. F. A. van der Vegt, and W. F. van Gunsteren, *Eur. Biophys. J.* **34**, 273 (2005).
- ⁴³A. J. Rzepiela, L. V. Schäfer, N. Goga, H. J. Risselada, A. H. de Vries, and S. J. Marrink, *J. Comput. Chem.* **31**, 1333 (2010).
- ⁴⁴D. Abramavicius, B. Palmieri, D. V. Voronine, F. Šanda, and S. Mukamel, *Chem. Rev.* **109**, 2350 (2009).
- ⁴⁵A. S. Davydov, *Sov. Phys. - Usp.* **7**, 145 (1964).
- ⁴⁶T. L. C. Jansen, B. M. Auer, M. Yang, and J. L. Skinner, *J. Chem. Phys.* **132**, 224503 (2010).
- ⁴⁷R. Tempelaar, T. L. C. Jansen, and J. Knoester, *J. Phys. Chem. B* **118**, 12865 (2014).
- ⁴⁸T. L. C. Jansen, S. Saito, J. Jeon, and M. Cho, *J. Chem. Phys.* **150**, 100901 (2019).
- ⁴⁹C. Olbrich, J. Strümpfer, K. Schulten, and U. Kleinekathöfer, *J. Phys. Chem. Lett.* **2**, 1771 (2011).
- ⁵⁰S. Valleau, A. Eisfeld, and A. Aspuru-Guzik, *J. Chem. Phys.* **137**, 224103 (2012).
- ⁵¹C. König and J. Neugebauer, *J. Phys. Chem. B* **117**, 3480 (2013).
- ⁵²S. Jurinovich, C. Curutchet, and B. Mennucci, *ChemPhysChem* **15**, 3194 (2014).
- ⁵³F. Segatta, L. Cupellini, S. Jurinovich, S. Mukamel, M. Dapor, S. Taioli, M. Garavelli, and B. Mennucci, *J. Am. Chem. Soc.* **139**, 7558 (2017).
- ⁵⁴S. Maity, B. M. Bold, J. D. Prajapati, M. Sokolov, T. Kubař, M. Elstner, and U. Kleinekathöfer, *J. Phys. Chem. Lett.* **11**, 8660 (2020).
- ⁵⁵C. R. Baiz, B. Błasiak, J. Bredenbeck, M. Cho, J.-H. Choi, S. A. Corcelli, A. G. Dijkstra, C.-J. Feng, S. Garrett-Roe, N.-H. Ge, M. W. D. Hanson-Heine, J. D. Hirst, T. L. C. Jansen, K. Kwac, K. J. Kubarych, C. H. Londergan, H. Maekawa, M. Reppert, S. Saito, S. Roy, J. L. Skinner, G. Stock, J. E. Straub, M. C. Thielges, K. Tominaga, A. Tokmakoff, H. Torii, L. Wang, L. J. Webb, and M. T. Zanni, *Chem. Rev.* **120**, 7152 (2020).
- ⁵⁶T. M. Watson and J. D. Hirst, *Mol. Phys.* **103**, 1531 (2005).
- ⁵⁷T. Hayashi, T. L. C. Jansen, W. Zhuang, and S. Mukamel, *J. Phys. Chem. A* **109**, 64 (2005).
- ⁵⁸S. A. Corcelli, C. P. Lawrence, and J. L. Skinner, *J. Chem. Phys.* **120**, 8107 (2004).
- ⁵⁹B. M. Auer and J. L. Skinner, *J. Chem. Phys.* **129**, 214705 (2008).
- ⁶⁰P. Bouř and T. A. Keiderling, *J. Chem. Phys.* **119**, 11253 (2003).
- ⁶¹K. Kwac and M. Cho, *J. Chem. Phys.* **119**, 2247 (2003).
- ⁶²T. L. C. Jansen and J. Knoester, *J. Chem. Phys.* **124**, 044502 (2006).
- ⁶³M. E. Madjet, A. Abdurahman, and T. Renger, *J. Phys. Chem. B* **110**, 17268 (2006).
- ⁶⁴A. S. Bondarenko, I. Patmanidis, R. Alessandri, P. C. T. Souza, T. L. C. Jansen, A. H. de Vries, S. J. Marrink, and J. Knoester, *Chem. Sci.* **11**, 11514 (2020).
- ⁶⁵R. Alessandri, S. Sami, J. Barnoud, A. H. de Vries, S. J. Marrink, and R. W. A. Havenith, *Adv. Funct. Mater.* **30**, 2004799 (2020).
- ⁶⁶S. Krimm and Y. Abe, *Proc. Natl. Acad. Sci. U. S. A.* **69**, 2788 (1972).
- ⁶⁷C. M. Baronio and A. Barth, *J. Phys. Chem. B* **124**, 1703 (2020).
- ⁶⁸A. Moran and S. Mukamel, *Proc. Natl. Acad. Sci. U. S. A.* **101**, 506 (2004).
- ⁶⁹S. Mukamel, *Principles of Nonlinear Optical Spectroscopy* (Oxford University Press, New York, 1995).
- ⁷⁰G. E. Uhlenbeck and L. S. Ornstein, *Phys. Rev.* **36**, 823 (1930).
- ⁷¹R. Kubo, *J. Phys. Soc. Jpn.* **17**, 1100 (1962).
- ⁷²N. G. van Kampen, *Stochastic Processes in Physics and Chemistry* (Elsevier BV, 1992).
- ⁷³C. Olbrich, J. Strümpfer, K. Schulten, and U. Kleinekathöfer, *J. Phys. Chem. B* **115**, 758 (2010).
- ⁷⁴C. P. Lawrence and J. L. Skinner, *J. Chem. Phys.* **117**, 8847 (2002).
- ⁷⁵Z. Wang, Y. Pang, and D. D. Dlott, *J. Chem. Phys.* **120**, 8345 (2004).
- ⁷⁶A. S. Bondarenko, J. Knoester, and T. L. C. Jansen, *Chem. Phys.* **529**, 110478 (2020).
- ⁷⁷D. Cringus, T. L. C. Jansen, M. S. Pshenichnikov, and D. A. Wiersma, *J. Chem. Phys.* **127**, 084507 (2007).
- ⁷⁸T. Ikeda and G. D. Scholes, *J. Chem. Phys.* **152**, 204101 (2020).
- ⁷⁹H. Liu, L. Zhu, S. Bai, and Q. Shi, *J. Chem. Phys.* **140**, 134106 (2014).
- ⁸⁰A. Ishizaki, *J. Phys. Soc. Jpn.* **89**, 015001 (2020).
- ⁸¹O. Rancova, M. Jakučiūnas, L. Valkunas, and D. Abramavicius, *Chem. Phys. Lett.* **674**, 120 (2017).
- ⁸²M. Dinpajoo and D. V. Matyushov, *J. Phys. Chem. B* **118**, 7925 (2014).
- ⁸³Y. S. Kim and R. M. Hochstrasser, *J. Phys. Chem. B* **111**, 9697 (2007).
- ⁸⁴K. Kwac, H. Lee, and M. Cho, *J. Chem. Phys.* **120**, 1477 (2004).
- ⁸⁵F. van Mourik, M. Chergui, and G. van der Zwan, *J. Phys. Chem. B* **105**, 9715 (2001).
- ⁸⁶T. L. C. Jansen, D. Cringus, and M. S. Pshenichnikov, *J. Phys. Chem. A* **113**, 6260 (2009).
- ⁸⁷S. Garrett-Roe and P. Hamm, *J. Chem. Phys.* **128**, 104507 (2008).
- ⁸⁸W. Zhuang, D. Abramavicius, R. Venkatramani, T. L. C. Jansen, D. Voronine, B. Robinson, T. Hayashi, and S. Mukamel, SPECTRON, <https://mukamel.ps.uci.edu/software.html>.
- ⁸⁹C. Liang and T. L. C. Jansen, *J. Chem. Theory Comput.* **8**, 1706 (2012).
- ⁹⁰See https://github.com/ghlacour/nise_2017 for NISE_2017.
- ⁹¹S. Mukamel, *Phys. Rev. A* **28**, 3480 (1983).
- ⁹²H. Torii, *J. Phys. Chem. A* **110**, 4822 (2006).
- ⁹³T. L. C. Jansen and J. Knoester, *J. Phys. Chem. B* **110**, 22910 (2006).
- ⁹⁴Y. Tanimura and R. Kubo, *J. Phys. Soc. Jpn.* **58**, 101 (1989).
- ⁹⁵A. Ishizaki and G. R. Fleming, *J. Chem. Phys.* **130**, 234111 (2009).
- ⁹⁶Y. Tanimura, *J. Chem. Phys.* **153**, 020901 (2020).
- ⁹⁷P. A. M. Dirac, *Proc. R. Soc. London, Ser. A* **114**, 243 (1927).
- ⁹⁸Y. R. Shen, *The Principles of Nonlinear Optics* (John Wiley & Sons, New York, 1984).
- ⁹⁹R. J. Boyd, *Nonlinear Optics* (Academic Press, San Diego, CA, 1992).
- ¹⁰⁰P. Hamm and M. T. Zanni, *Concepts and Methods of 2D Infrared Spectroscopy* (Cambridge University Press, Cambridge, 2011).
- ¹⁰¹J. R. Schmidt, S. A. Corcelli, and J. L. Skinner, *J. Chem. Phys.* **123**, 044513 (2005).
- ¹⁰²H. Torii and M. Tasumi, *J. Chem. Phys.* **99**, 8459 (1993).
- ¹⁰³H. Torii, *J. Mol. Struct.: THEOCHEM* **311**, 199 (1994).
- ¹⁰⁴K. F. Everitt and J. L. Skinner, *Chem. Phys.* **266**, 197 (2001).
- ¹⁰⁵K. F. Everitt, E. Geva, and J. L. Skinner, *J. Chem. Phys.* **114**, 1326 (2001).
- ¹⁰⁶A. Piryatinski, C. P. Lawrence, and J. L. Skinner, *J. Chem. Phys.* **118**, 9664 (2003).
- ¹⁰⁷A. Piryatinski, C. P. Lawrence, and J. L. Skinner, *J. Chem. Phys.* **118**, 9672 (2003).
- ¹⁰⁸M. Cho, *Two-Dimensional Optical Spectroscopy* (CRC Press, Boca Raton, FL, 2009).
- ¹⁰⁹C. P. van der Vegte, A. G. Dijkstra, J. Knoester, and T. L. C. Jansen, *J. Phys. Chem. A* **117**, 5970 (2013).

- ¹¹⁰C. P. van der Vegte, S. Knop, P. Vöhringer, J. Knoester, and T. L. C. Jansen, *J. Phys. Chem. B* **118**, 6256 (2014).
- ¹¹¹C. P. van der Vegte, J. D. Prajapati, U. Kleinekathöfer, J. Knoester, and T. L. C. Jansen, *J. Phys. Chem. B* **119**, 1302 (2015).
- ¹¹²P. L. McRobbie, G. Hanna, Q. Shi, and E. Geva, *Acc. Chem. Res.* **42**, 1299 (2009).
- ¹¹³G. Hanna and E. Geva, *J. Phys. Chem. B* **113**, 9278 (2009).
- ¹¹⁴M. Tsuchimoto and Y. Tanimura, *J. Chem. Theory Comput.* **11**, 3859 (2015).
- ¹¹⁵J. Strümpfer and K. Schulten, *J. Chem. Theory Comput.* **8**, 2808 (2012).
- ¹¹⁶C. Kreisbeck, T. Kramer, M. Rodríguez, and B. Hein, *J. Chem. Theory Comput.* **7**, 2166 (2011).
- ¹¹⁷L. Chen, R. Zheng, Q. Shi, and Y. Yan, *J. Chem. Phys.* **132**, 024505 (2010).
- ¹¹⁸J. Xu, R.-x. Xu, D. Abramavicius, H.-d. Zhang, and Y.-j. Yan, *Chin. J. Chem. Phys.* **24**, 497 (2011).
- ¹¹⁹A. Ishizaki and Y. Tanimura, *J. Phys. Soc. Jpn.* **74**, 3131 (2005).
- ¹²⁰A. Ishizaki and Y. Tanimura, *J. Chem. Phys.* **125**, 084501 (2006).
- ¹²¹A. Ishizaki and Y. Tanimura, *J. Phys. Chem. A* **111**, 9269 (2007).
- ¹²²A. Sakurai and Y. Tanimura, *J. Phys. Chem. A* **115**, 4009 (2011).
- ¹²³J.-J. Ding, J. Xu, J. Hu, R.-X. Xu, and Y. Yan, *J. Chem. Phys.* **135**, 164107 (2011).
- ¹²⁴B. Hein, C. Kreisbeck, T. Kramer, and M. Rodríguez, *New J. Phys.* **14**, 023018 (2012).
- ¹²⁵P. Kjellberg, B. Brüggeman, and T. Pullerits, *Phys. Rev. B* **74**, 024303 (2006).
- ¹²⁶H.-G. Duan, P. Nalbach, V. I. Prokhorenko, S. Mukamel, and M. Thorwart, *New J. Phys.* **17**, 072002 (2015).
- ¹²⁷R. M. Stratt, *Acc. Chem. Res.* **28**, 201 (1995).
- ¹²⁸T. Keyes and J. T. Fourkas, *J. Chem. Phys.* **112**, 287 (2000).
- ¹²⁹T. L. C. Jansen, J. G. Snijders, and K. Duppen, *J. Chem. Phys.* **113**, 307 (2000).
- ¹³⁰T. L. C. Jansen and S. Mukamel, *J. Chem. Phys.* **119**, 7979 (2003).
- ¹³¹T. Yagasaki and S. Saito, *J. Chem. Phys.* **128**, 154521 (2008).
- ¹³²R. F. Loring, *J. Chem. Phys.* **146**, 144106 (2017).
- ¹³³M. Kasha, *Radiat. Res.* **20**, 55 (1963).
- ¹³⁴N. J. Hestand and F. C. Spano, *Chem. Rev.* **118**, 7069 (2018).
- ¹³⁵T. L. C. Jansen, *Chem* **5**, 3010 (2019).
- ¹³⁶C. Chuang, D. I. G. Bennett, J. R. Caram, A. Aspuru-Guzik, M. G. Bawendi, and J. Cao, *Chem* **5**, 3135 (2019).
- ¹³⁷C. Didraga, J. A. Klugkist, and J. Knoester, *J. Phys. Chem. B* **106**, 11474 (2002).
- ¹³⁸A. Löhner, T. Kunsel, M. I. S. Röhr, T. L. C. Jansen, S. Sengupta, F. Würthner, J. Knoester, and J. Köhler, *J. Phys. Chem. Lett.* **10**, 2715 (2019).
- ¹³⁹L. M. Günther, A. Löhner, C. Reiher, T. Kunsel, T. L. C. Jansen, M. Tank, D. A. Bryant, J. Knoester, and J. Köhler, *J. Phys. Chem. B* **122**, 6712 (2018).
- ¹⁴⁰A. Rodger, G. Dorrington, and D. L. Ang, *Analyst* **141**, 6490 (2016).
- ¹⁴¹D. Lindorfer and T. Renger, *J. Phys. Chem. B* **122**, 2747 (2018).
- ¹⁴²A. P. H. J. Schenning, P. Jonkheijm, E. Peeters, and E. W. Meijer, *J. Am. Chem. Soc.* **123**, 409 (2001).
- ¹⁴³R. Tempelaar, A. Stradomska, J. Knoester, and F. C. Spano, *J. Phys. Chem. B* **115**, 10592 (2011).
- ¹⁴⁴Y. Dorca, E. E. Greciano, J. S. Valera, R. Gómez, and L. Sánchez, *Chem. Eur. J.* **25**, 5848 (2019).
- ¹⁴⁵Y. Tanimura and S. Mukamel, *J. Chem. Phys.* **99**, 9496 (1993).
- ¹⁴⁶J. Bredenbeck, A. Ghosh, M. Smits, and M. Bonn, *J. Am. Chem. Soc.* **130**, 2152 (2008).
- ¹⁴⁷W. Xiong, J. E. Laaser, R. D. Mehlenbacher, and M. T. Zanni, *Proc. Natl. Acad. Sci. U. S. A.* **108**, 20902 (2011).
- ¹⁴⁸O. Golonzka, M. Khalil, N. Demirdöven, and A. Tokmakoff, *J. Chem. Phys.* **115**, 10814 (2001).
- ¹⁴⁹T. L. C. Jansen and J. Knoester, *Biophys. J.* **94**, 1818 (2008).
- ¹⁵⁰K. J. Gaffney, I. R. Piletic, and M. D. Fayer, *J. Chem. Phys.* **118**, 2270 (2003).
- ¹⁵¹L. J. G. W. van Wilderen and J. Bredenbeck, *Angew. Chem., Int. Ed.* **54**, 11624 (2015).
- ¹⁵²J. Dostál, F. Fennel, F. Koch, S. Herbst, F. Würthner, and T. Brixner, *Nat. Commun.* **9**, 2466 (2018).
- ¹⁵³S. Draeger, S. Roeding, and T. Brixner, *Opt. Express* **25**, 3259 (2017).
- ¹⁵⁴A. A. Bakulin, A. Rao, V. G. Pavelyev, P. H. M. van Loosdrecht, M. S. Pshenichnikov, D. Niedzialek, J. Cornil, D. Beljonne, and R. H. Friend, *Science* **335**, 1340 (2012).
- ¹⁵⁵A. Loukianov, A. Niedringhaus, B. Berg, J. Pan, S. S. Senlik, and J. P. Ogilvie, *J. Phys. Chem. Lett.* **8**, 679 (2017).
- ¹⁵⁶E. Harel, *J. Chem. Phys.* **146**, 154201 (2017).
- ¹⁵⁷S. Garrett-Roe and P. Hamm, *J. Chem. Phys.* **130**, 164510 (2009).
- ¹⁵⁸K. J. Kubarych, C. J. Milne, and R. J. D. Miller, *Chem. Phys. Lett.* **369**, 635 (2003).
- ¹⁵⁹P. F. Tekavec, G. A. Lott, and A. H. Marcus, *J. Chem. Phys.* **127**, 214307 (2007).
- ¹⁶⁰Z. W. Fox, T. J. Blair, and M. Khalil, *J. Phys. Chem. Lett.* **11**, 1558 (2020).
- ¹⁶¹N. Zhou, Z. Ouyang, J. Hu, O. F. Williams, L. Yan, W. You, and A. M. Moran, *J. Phys. Chem. Lett.* **11**, 4570 (2020).
- ¹⁶²C. Falvo, B. Palmieri, and S. Mukamel, *J. Chem. Phys.* **130**, 184501 (2009).
- ¹⁶³A. Paarmann, T. Hayashi, S. Mukamel, and R. J. D. Miller, *J. Chem. Phys.* **130**, 204110 (2009).
- ¹⁶⁴M. F. DeCamp, L. DeFlores, J. M. McCracken, A. Tokmakoff, K. Kwac, and M. Cho, *J. Phys. Chem. B* **109**, 11016 (2005).
- ¹⁶⁵H. Torii and M. Tasumi, *J. Chem. Phys.* **96**, 3379 (1992).
- ¹⁶⁶E. Małolepsza and J. E. Straub, *J. Phys. Chem. B* **118**, 7848 (2014).
- ¹⁶⁷E.-L. Karjalainen, T. Ersmark, and A. Barth, *J. Phys. Chem. B* **116**, 4831 (2012).
- ¹⁶⁸A. S. Bondarenko and T. L. C. Jansen, *J. Phys. Chem.* **142**, 212437 (2015).
- ¹⁶⁹A. V. Cunha, A. S. Bondarenko, and T. L. C. Jansen, *J. Chem. Theory Comput.* **12**, 3982 (2016).
- ¹⁷⁰L. P. DeFlores and A. Tokmakoff, *J. Am. Chem. Soc.* **128**, 16520 (2006).
- ¹⁷¹E. B. Dunkelberger, A. M. Woys, and M. T. Zanni, *J. Phys. Chem. B* **117**, 15297 (2013).
- ¹⁷²E. Palacino-González, M. F. Gelin, and W. Domcke, *J. Chem. Phys.* **150**, 204102 (2019).
- ¹⁷³V. Andruschenko, P. Matejka, D. T. Anderson, J. Kaminskiy, J. Hornicek, L. O. Paulson, and P. Bour, *J. Phys. Chem. A* **113**, 9727 (2009).
- ¹⁷⁴S. Jakobsen, T. Bereau, and M. Meuwly, *J. Phys. Chem. B* **119**, 3034 (2015).
- ¹⁷⁵Y. Mu, D. S. Kosov, and G. Stock, *J. Phys. Chem. B* **107**, 5064 (2003).
- ¹⁷⁶S. Imoto, S. S. Xantheas, and S. Saito, *J. Chem. Phys.* **139**, 044503 (2013).
- ¹⁷⁷T. Hasegawa and Y. Tanimura, *J. Phys. Chem. B* **115**, 5545 (2011).
- ¹⁷⁸T. L. C. Jansen, *J. Phys. Chem. B* **118**, 8162 (2014).
- ¹⁷⁹C. J. Tainter, P. A. Pieniazek, Y.-S. Lin, and J. L. Skinner, *J. Chem. Phys.* **134**, 184501 (2011).
- ¹⁸⁰G. R. Medders and F. Paesani, *J. Chem. Theory Comput.* **11**, 1145 (2015).
- ¹⁸¹R. B. Gerber, G. M. Chaban, S. K. Gregurick, and B. Brauer, *Biopolymers* **68**, 370 (2003).
- ¹⁸²S. Chandrasekaran, M. Aghtar, S. Valteau, A. Aspuru-Guzik, and U. Kleinekathöfer, *J. Phys. Chem. B* **119**, 9995 (2015).
- ¹⁸³E. Harder, V. M. Anisimov, T. Whitfield, A. D. MacKerell, and B. Roux, *J. Phys. Chem. B* **112**, 3509 (2008).
- ¹⁸⁴K. A. Beauchamp, Y.-S. Lin, R. Das, and V. S. Pande, *J. Chem. Theory Comput.* **8**, 1409 (2012).
- ¹⁸⁵J. Manor, P. Mukherjee, Y.-S. Lin, H. Leonov, J. L. Skinner, M. T. Zanni, and I. T. Arkin, *Structure* **17**, 247 (2009).
- ¹⁸⁶A. Ghosh, J. Qiu, W. F. DeGrado, and R. M. Hochstrasser, *Proc. Natl. Acad. Sci. U. S. A.* **108**, 6115 (2011).
- ¹⁸⁷M. Reppert, A. R. Roy, J. O. B. Tempkin, A. R. Dinner, and A. Tokmakoff, *J. Phys. Chem. B* **120**, 11395 (2016).
- ¹⁸⁸O. Selig, A. V. Cunha, M. B. van Eldijk, J. C. M. van Hest, T. L. C. Jansen, H. J. Bakker, and Y. L. A. Rezus, *J. Phys. Chem. B* **122**, 8243 (2018).
- ¹⁸⁹Y. El Khoury, G. Le Breton, A. V. Cunha, T. L. C. Jansen, L. J. G. W. van Wilderen, and J. Bredenbeck, *J. Chem. Phys.* **154**, 124201 (2021).

- ¹⁹⁰H. T. Kratochvil, J. K. Carr, K. Matulef, A. W. Annen, H. Li, M. Maj, J. Ostmeyer, A. L. Serrano, H. Raghuraman, S. D. Moran, J. L. Skinner, E. Perozo, B. Roux, F. I. Valiyaveetil, and M. T. Zanni, *Science* **353**, 1040 (2016).
- ¹⁹¹W. Kopec, D. A. Köpfer, O. N. Vickery, A. S. Bondarenko, T. L. C. Jansen, B. L. de Groot, and U. Zachariae, *Nat. Chem.* **10**, 813 (2018).
- ¹⁹²S. E. Strong, N. J. Hestand, A. A. Kananenka, M. T. Zanni, and J. Skinner, *Biophys. J.* **118**, 254 (2019).
- ¹⁹³X. Li, F. Buda, H. J. M. de Groot, and G. J. A. Sevink, *J. Phys. Chem. C* **123**, 16462 (2019).
- ¹⁹⁴T. Kunsel, A. Löhner, J. J. Mayo, J. Köhler, T. L. C. Jansen, and J. Knoester, *J. Chem. Phys.* **153**, 134304 (2020).
- ¹⁹⁵J. Megow, M. I. S. Röhr, M. Schmidt am Busch, T. Renger, R. Mitrić, S. Kirstein, J. P. Rabe, and V. May, *Phys. Chem. Chem. Phys.* **17**, 6741 (2015).
- ¹⁹⁶D. J. Thouless, *Phys. Rep.* **13**, 93 (1974).
- ¹⁹⁷P. D. Reilly and J. L. Skinner, *Phys. Rev. Lett.* **71**, 4257 (1993).
- ¹⁹⁸L. D. Bakalis and J. Knoester, *J. Phys. Chem. B* **103**, 6620 (1999).
- ¹⁹⁹A. S. Bondarenko, T. L. C. Jansen, and J. Knoester, *J. Chem. Phys.* **152**, 194302 (2020).
- ²⁰⁰C. Didraga and J. Knoester, *J. Chem. Phys.* **121**, 10687 (2004).
- ²⁰¹A. G. Dijkstra, T. L. C. Jansen, and J. Knoester, *J. Chem. Phys.* **128**, 164511 (2008).
- ²⁰²P. Debye, *Ann. Phys.* **348**, 49 (1913).
- ²⁰³J. L. Yarnell, M. J. Katz, R. G. Wenzel, and S. H. Koenig, *Phys. Rev. A* **7**, 2130 (1973).
- ²⁰⁴A. V. Cunha, E. Salamatova, R. Bloem, S. J. Roeters, S. Woutersen, M. S. Pshenichnikov, and T. L. C. Jansen, *J. Phys. Chem. Lett.* **8**, 2438 (2017).
- ²⁰⁵D. M. Jonas, M. J. Lang, Y. Nagasawa, T. Joo, and G. R. Fleming, *J. Phys. Chem.* **100**, 12660 (1996).
- ²⁰⁶H. J. Bakker, S. Woutersen, and H.-K. Nienhuys, *Chem. Phys.* **258**, 233 (2000).
- ²⁰⁷M. Ji and K. J. Gaffney, *J. Chem. Phys.* **134**, 044516 (2011).
- ²⁰⁸A. A. Bakulin, O. Selig, H. J. Bakker, Y. L. A. Rezus, C. Müller, T. Glaser, R. Lovrincic, Z. Sun, Z. Chen, A. Walsh, J. M. Frost, and T. L. C. Jansen, *J. Phys. Chem. Lett.* **6**, 3663 (2015).
- ²⁰⁹S. Woutersen and P. Hamm, *J. Phys. Chem. B* **104**, 11316 (2000).
- ²¹⁰M. T. Zanni, N.-H. Ge, Y. S. Kim, and R. M. Hochstrasser, *Proc. Natl. Acad. Sci. U. S. A.* **98**, 11265 (2001).
- ²¹¹S. Woutersen and H. J. Bakker, *Nature* **402**, 507 (1999).
- ²¹²S. C. Massey, P.-C. Ting, S.-H. Yeh, P. D. Dahlberg, S. H. Sohail, M. A. Allodi, E. C. Martin, S. Kais, C. N. Hunter, and G. S. Engel, *J. Phys. Chem. Lett.* **10**, 270 (2019).
- ²¹³G. D. Scholes, G. R. Fleming, L. X. Chen, A. Aspuru-Guzik, A. Buchleitner, D. F. Coker, G. S. Engel, R. van Grondelle, A. Ishizaki, D. M. Jonas, J. S. Lundeen, J. K. McCusker, S. Mukamel, J. P. Ogilvie, A. Olaya-Castro, M. A. Ratner, F. C. Spano, K. B. Whaley, and X. Zhu, *Nature* **543**, 647 (2017).
- ²¹⁴J. Cao, R. J. Cogdell, D. F. Coker, H.-G. Duan, J. Hauer, U. Kleinekathöfer, T. L. C. Jansen, T. Mančal, R. J. D. Miller, J. P. Ogilvie *et al.*, *Sci. Adv.* **6**, eaaz4888 (2020).
- ²¹⁵J. Adolphs and T. Renger, *Biophys. J.* **91**, 2778 (2006).
- ²¹⁶A. G. Dijkstra and Y. Tanimura, *New J. Phys.* **14**, 073027 (2012).
- ²¹⁷T. Fujita, J. Huh, S. K. Saikin, J. C. Brookes, and A. Aspuru-Guzik, *Photosynth. Res.* **120**, 273 (2014).
- ²¹⁸S. Valteau, S. K. Saikin, D. Ansari-Oghol-Beig, M. Rostami, H. Mossallaei, and A. Aspuru-Guzik, *ACS Nano* **8**, 3884 (2014).
- ²¹⁹T. Kramer, M. Noack, J. R. Reimers, A. Reinefeld, M. Rodriguez, and S. Yin, *Chem. Phys.* **515**, 262 (2018).
- ²²⁰J.-H. Choi, H. Lee, K.-K. Lee, S. Hahn, and M. Cho, *J. Chem. Phys.* **126**, 045102 (2007).
- ²²¹J. Jeon, S. Yang, J.-H. Choi, and M. Cho, *Acc. Chem. Res.* **42**, 1280 (2009).
- ²²²S. Woutersen and P. Hamm, *J. Chem. Phys.* **115**, 7737 (2001).
- ²²³H. Maekawa, F. Formaggio, C. Toniolo, and N.-H. Ge, *J. Am. Chem. Soc.* **130**, 6556 (2008).
- ²²⁴C. M. Cheatum, A. Tokmakoff, and J. Knoester, *J. Chem. Phys.* **120**, 8201 (2004).
- ²²⁵A. A. Adzhubei, M. J. E. Sternberg, and A. A. Makarov, *J. Mol. Biol.* **425**, 2100 (2013).
- ²²⁶B. L. Pentelute, Z. P. Gates, V. Tereshko, J. L. Dashnau, J. M. Vanderkooi, A. A. Kossiakoff, and S. B. H. Kent, *J. Am. Chem. Soc.* **130**, 9695 (2008).
- ²²⁷L. Verlet, *Phys. Rev.* **159**, 98 (1967).
- ²²⁸U. Essmann, L. Perera, M. L. Berkowitz, T. Darden, H. Lee, and L. G. Pedersen, *J. Chem. Phys.* **103**, 8577 (1995).
- ²²⁹G. Bussi, D. Donadio, and M. Parrinello, *J. Chem. Phys.* **126**, 014101 (2007).
- ²³⁰M. Parrinello and A. Rahman, *J. Appl. Phys.* **52**, 7182 (1981).
- ²³¹M. J. Abraham, T. Murtola, R. Schulz, S. Páll, J. C. Smith, B. Hess, and E. Lindahl, *SoftwareX* **1-2**, 19 (2015).
- ²³²G. N. Ramachandran, C. Ramakrishnan, and V. Sasisekharan, *J. Mol. Biol.* **7**, 95 (1963).
- ²³³N. Michaud-Agrawal, E. J. Denning, T. B. Woolf, and O. Beckstein, *J. Comput. Chem.* **32**, 2319 (2011).
- ²³⁴See <https://github.com/ghlacour/amideimaps> for computer code for extracting amide I Hamiltonian.
- ²³⁵T. L. C. Jansen, A. G. Dijkstra, T. M. Watson, J. D. Hirst, and J. Knoester, *J. Chem. Phys.* **125**, 044312 (2006).
- ²³⁶S. Roy, J. Lessing, G. Meisl, Z. Ganim, A. Tokmakoff, J. Knoester, and T. L. C. Jansen, *J. Chem. Phys.* **135**, 234507 (2011).
- ²³⁷S. Woutersen and P. Hamm, *J. Chem. Phys.* **114**, 2727 (2001).
- ²³⁸Y.-S. Lin, J. M. Shorb, P. Mukherjee, M. T. Zanni, and J. L. Skinner, *J. Phys. Chem. B* **113**, 592 (2009).
- ²³⁹A. G. Dijkstra and J. Knoester, *J. Phys. Chem. B* **109**, 9787 (2005).
- ²⁴⁰S. M. Prince, M. Z. Papiz, A. A. Freer, G. McDermott, A. M. Hawthornthwaite-Lawless, R. J. Cogdell, and N. W. Isaacs, *J. Mol. Biol.* **268**, 412 (1997).
- ²⁴¹S. Georgakopoulou, R. N. Frese, E. Johnson, C. Koolhaas, R. J. Cogdell, R. van Grondelle, and G. van der Zwan, *Biophys. J.* **82**, 2184 (2002).
- ²⁴²K. Sauer, R. J. Cogdell, S. M. Prince, A. Freer, N. W. Isaacs, and H. Scheer, *Photochem. Photobiol.* **64**, 564 (1996).
- ²⁴³O. Rancova, J. Sulskus, and D. Abramavicius, *J. Phys. Chem. B* **116**, 7803 (2012).
- ²⁴⁴M. V. Mostovoy and J. Knoester, *J. Phys. Chem. B* **104**, 12355 (2000).
- ²⁴⁵G. Trinkunas, J. L. Herek, T. Polívka, V. Sundström, and T. Pullerits, *Phys. Rev. Lett.* **86**, 4167 (2001).
- ²⁴⁶A. F. Fidler, V. P. Singh, P. D. Long, P. D. Dahlberg, and G. S. Engel, *J. Chem. Phys.* **139**, 155101 (2013).
- ²⁴⁷M. Ferretti, R. Hendrikx, E. Romero, J. Southall, R. J. Cogdell, V. I. Novoderezhkin, G. D. Scholes, and R. van Grondelle, *Sci. Rep.* **6**, 20834 (2016).
- ²⁴⁸O. Rancova and D. Abramavicius, *J. Phys. Chem. B* **118**, 7533 (2014).
- ²⁴⁹See https://github.com/ghlacour/nise_tutorials for NISE_Tutorials.
- ²⁵⁰R. Ramakrishnan, P. O. Dral, M. Rupp, and O. A. von Lilienfeld, *J. Chem. Theory Comput.* **11**, 2087 (2015).
- ²⁵¹N. Artrith, K. T. Butler, F.-X. Coudert, S. Han, O. Isayev, A. Jain, and A. Walsh, *Nat. Chem.* **13**, 505 (2021).
- ²⁵²S. Ye, W. Hu, X. Li, J. Zhang, K. Zhong, G. Zhang, Y. Luo, S. Mukamel, and J. Jiang, *Proc. Natl. Acad. Sci. U. S. A.* **116**, 11612 (2019).
- ²⁵³A. A. Kananenka, K. Yao, S. A. Corcelli, and J. L. Skinner, *J. Chem. Theory Comput.* **15**, 6850 (2019).
- ²⁵⁴K. Kwac and M. Cho, *J. Chem. Phys.* **152**, 174101 (2020).
- ²⁵⁵S. Ye, K. Zhong, J. Zhang, W. Hu, J. D. Hirst, G. Zhang, S. Mukamel, and J. Jiang, *J. Am. Chem. Soc.* **142**, 19071 (2020).
- ²⁵⁶M. S. Chen, T. J. Zuehlsdorff, T. Morawietz, C. M. Isborn, and T. E. Markland, *J. Phys. Chem. Lett.* **11**, 7559 (2020).
- ²⁵⁷M. Rodríguez and T. Kramer, *Chem. Phys.* **520**, 52 (2019).
- ²⁵⁸A. Sisto, C. Stross, M. W. van der Kamp, M. O'Connor, S. McIntosh-Smith, G. T. Johnson, E. G. Hohenstein, F. R. Manby, D. R. Glowacki, and T. J. Martinez, *Phys. Chem. Chem. Phys.* **19**, 14924 (2017).
- ²⁵⁹C. Kreisbeck and T. Kramer, *J. Phys. Chem. Lett.* **3**, 2828 (2012).
- ²⁶⁰A. Teplukhin, B. K. Kendrick, and D. Babikov, *J. Chem. Theory Comput.* **15**, 4555 (2019).

- ²⁶¹F. Arute, K. Arya, R. Babbush, D. Bacon, J. C. Bardin, R. Barends, R. Biswas, S. Boixo, F. G. S. L. Brandao, D. A. Buell *et al.*, *Nature* **574**, 505 (2019).
- ²⁶²M. Levitt, *Angew. Chem., Int. Ed.* **53**, 10006 (2014).
- ²⁶³S. J. Marrink, H. J. Risselada, S. Yefimov, D. P. Tieleman, and A. H. de Vries, *J. Phys. Chem. B* **111**, 7812 (2007).
- ²⁶⁴C. Liang and T. L. C. Jansen, *J. Phys. Chem. B* **117**, 6937 (2013).
- ²⁶⁵H. Zhou and D. I. G. Bennett, *J. Chem. Phys.* **151**, 144112 (2019).
- ²⁶⁶L. Varvelo, J. K. Lynd, and D. I. G. Bennett, [arXiv:2008.06496](https://arxiv.org/abs/2008.06496) (2020).
- ²⁶⁷L. Varvelo, J. K. Lynd, and D. I. G. Bennett, *Chem. Sci.* **12**, 9704 (2021).
- ²⁶⁸H. Sumi, *J. Phys. Chem. B* **103**, 252 (1999).
- ²⁶⁹A. Mandal and A. Tokmakoff, *J. Chem. Phys.* **143**, 194501 (2015).
- ²⁷⁰N. M. Kearns, R. D. Mehlenbacher, A. C. Jones, and M. T. Zanni, *Opt. Express* **25**, 7869 (2017).
- ²⁷¹M. Son, S. Mosquera-Vázquez, and G. S. Schlau-Cohen, *Opt. Express* **25**, 18950 (2017).
- ²⁷²J. D. Gaynor, J. Sandwisch, and M. Khalil, *Nat. Commun.* **10**, 5621 (2019).
- ²⁷³M. Cho and G. R. Fleming, *J. Phys. Chem. B* **124**, 11222 (2020).
- ²⁷⁴N. H. C. Lewis, H. Dong, T. A. A. Oliver, and G. R. Fleming, *J. Chem. Phys.* **143**, 124203 (2015).
- ²⁷⁵H. Dong, N. H. C. Lewis, T. A. A. Oliver, and G. R. Fleming, *J. Chem. Phys.* **142**, 174201 (2015).
- ²⁷⁶N. H. C. Lewis, H. Dong, T. A. A. Oliver, and G. R. Fleming, *J. Chem. Phys.* **142**, 174202 (2015).
- ²⁷⁷P. Bhattacharyya and G. R. Fleming, *J. Phys. Chem. Lett.* **10**, 2081 (2019).
- ²⁷⁸G. A. Lott, A. Perdomo-Ortiz, J. K. Utterback, J. R. Widom, A. Aspuru-Guzik, and A. H. Marcus, *Proc. Natl. Acad. Sci. U. S. A.* **108**, 16521 (2011).